#### MINISTRY OF NATIONAL EDUCATION AND SCIENTIFIC RESEARCH TECHNICAL UNIVERSITY OF CIVIL ENGINEERING BUCHAREST DOCTORAL SCHOOL

Research Raport No. 1

# Simulation of Ground Motions Generated by Vrancea Intermediate-Depth Seismic Source. Results Interpretation. Pros and Cons

PhD Supervisor:

Prof. PhD.eng. Radu VACAREANU

PhD Student:

eng. Eliza-Anabella COŢOVANU

#### Table of contents

List of figures	. 3
List of tables	. 5
1. Introduction	. 6
2. Empirical Green's function method	. 8
3. Stochastic simulations	11
4. Physical based numerical modeling. Theoretical simulations (3D)	17
5. Hybrid methods	18
6. Simulations of the ground motion generated by the intermediate depth earthquake in October 27, 2004 at INCERC station. Interpretation of results	
6.1. Earthquake characteristics	19
6.2. The first set of simulations	20
Input data	20
Modified parameter (calibration)	22
Interpretation of results	23
6.3. The second set of simulations. SMSIM simulations without the influence of local site conditions	26
6.4. The third set of simulations. SMSIM simulations near source	
6.5. The fourth set of simulations. SMSIM simulations near source for a stress drop of 75 ba and one of 200 bars	rs
6.6. The fifth set of simulations	29
6.7. The sixth set of simulations. Window function	30
6.8. Final set of simulations	34
7. Simulations of the ground motion generated by the intermediate depth earthquake in August 30, 1986 at INCERC station. Interpretation of results	36
7.1. Earthquake characteristics	36
7.2. Input parameters	36
7.3. Characteristics of simulations	37
8. Conclusion. Pros and cons	40
Biography	41

#### List of figures

Figure 1 Schematic illustration of the Green's empirical function method. (a) Fault areas (small and large). (b) Filter to adjust to the difference in slip velocity function between the large and small events according to Irikura 1986 (the function is a sum between a delta and boxcar function). (c) Filter modified according to Irikura et al. 1997 with an exponential function instead of a boxcar function where T is the risetime for the large event. (d) Schematic displacement amplitude spectra following the omega-squared source scaling model, assuming a stress drop ratio C between the large and small events. (e) Acceleration amplitude spectra following the omega-squared source scaling model (Lecture Note on Strong Motion Figure 2. The principle of obtaining the simulated accelerograms using the finite source Figure 3. The combined effect of the site (taking into account both amplification and Figure 4. Example of spatial grid used in simulations with numerical methods (Irikura and Figure 5. Hybrid seismic motion simulation method for large earthquakes (Irikura and Figure 6. Examples of filters used in hybrid method and example of large earthquake Figure 7. The faults dimensions of the earthquake October 27, 2004, August 30, 1986, and Figure 8. Variation of peak accelerations within the sets of 400 simulations for each of the 4 Figure 9. Variation of peak accelerations in the 400 simulations performed for the three source types and 2 local amplification types (the PAGs values were ordinated for a better Figure 10. Cumulative energies of actual records and simulations with SMSIM Energiile Figure 11. Comparison between the normalized response spectra of the simulations and of the ground motions recorded during the earthquake of October 27, 2004 at INCERC station ..... 25 Figure 12. Comparison of the response spectra of simulations made with source S1 and of the ground motions recorded during the earthquake of October 27, 2004 at INCERC station ..... 25 Figure 13. Comparison of the response spectra of simulations made with source S11 and of the ground motions recorded during the earthquake of October 27, 2004 at INCERC station 26 Figure 14. Comparison of the response spectra of simulations made with source S12 and of the ground motions recorded during the earthquake of October 27, 2004 at INCERC station 26 Figure 15. Comparison of normalized response spectra of simulations without the influence of local site conditions and of the ground motions recorded during the earthquake of October 27, Figure 16. Comparison of normalized response spectra of simulations near the source and of the ground motions recorded during the earthquake of October 27, 2004 at INCERC station 27 Figure 18. Comparison of the normalized response spectra of simulations near the source with stress drops of 75 bars and 200 bars and of the ground motions recorded during the Figure 19. Comparison of the normalized response spectra of S12 simulations near the source with stress drops of 75 bars and 200 bars and of the ground motions recorded during the 

Figure 20. Comparison of the normalized response spectra of S11 simulations near the source
with stress drops of 75 bars and 200 bars and of the ground motions recorded during the
earthquake of October 27, 2004 at INCERC station
Figure 21. Comparison between the simulated response spectra using source S12, geometric
scattering 0.4 and path duration 0.09 and of the ground motions recorded during the
earthquake of October 27, 2004 at INCERC station
Figure 22. Comparison between the cumulative energies of simulations and those of the
ground motions recorded during the earthquake of October 27, 2004 at INCERC station 30
Figure 23. Comparison between the cumulative energies of simulations with different
parameters for the window and those of the ground motions recorded during the earthquake of
October 27, 2004 at INCERC station (first part)
Figure 24 Comparison between the cumulative energies of simulations with different
parameters for the window and those of the ground motions recorded during the earthquake of
October 27, 2004 at INCERC station (second part)32
Figure 25. Comparison between the simulated accelerograms using window 16 and 24 and the
NS INCERC accelerogram recorded on October 27, 2004
Figure 26. Normalized accelerogram simulated with window 24
Figure 27. NS INCERC normalized accelerogram recorded on 27 octombrie 2004 33
Figure 28. Normalized accelerogram simulated with window 16
Figure 29. Comparison between the simulated cumulative energies of the final version and
those of the ground motions recorded during the earthquake of October 27, 2004 at INCERC
station
Figure 30. Comparison of the response spectra of simulated accelerograms and those of the
ground motions recorded during the earthquake of October 27, 2004 at INCERC station 35
Figure 31. Comparison of the response spectra of simulated accelerograms and those of the
ground motions recorded during the earthquake of October 27, 2004 at INCERC station 35
Figure 32. Comparison of the response spectra of simulated accelerograms and those of the
ground motions recorded during the earthquake of October 27, 2004 at INCERC station 35
Figure 34. Cumulative energies of recorded ground motions and simulations made with
SMSIM with NRATTLE and H/V soil profile amplification
Figure 35. Comparison of the response spectra of simulations made with SMSIM source S1
and of recorded ground motions on August 30, 1986's Vrancea earthquake, INCERC seismic
station
Figure 36. Comparison of the response spectra of simulations made with SMSIM source S11
and of recorded ground motions on August 30, 1986's Vrancea earthquake, INCERC seismic
station
Figure 37. Comparison of the response spectra of simulations made with SMSIM source S12
and of recorded ground motions on August 30, 1986's Vrancea earthquake, INCERC seismic
station

#### List of tables

Table 1 Spectrum types for source definition (Boore, 2003)	14
Table 2 Average peak acceleration for different stress values	22
Table 3. Characteristics of simulated ground motion of October 27, 2004 for a 200 bar	stress
drop	23
Table 4. The characteristics of the simulated motions for a stress drop of 75 bars	30
Table 5. Types of window parameters	31
Table 6. Characteristics of simulated ground motion of 27 October 2004 for a 75 bars	stress
drop, geometric spreading of 0.4 and path time 0.09	36
Table 7. Characteristics of simulated ground motion of August 1986's earthquake	using
SMSIM	37

5

#### 1. Introduction

The seismic hazard in Romania is given by the intermediate-depth seismic source Vrancea and by the crustal seismogenic areas, distributed throughout the country: Făgăraş - Câmpulung, Danubian area, Banat, Crişana - Maramureş, Bârlad depression, Transobrogean depression (Radulian et al., 2000).

The Vrancea seismogenic source is at the convergence of three tectonic units: the East-European plate, the Intra-Alpine subplate and Moesic subplate (Constantinescu et al., 1976), this covers an epicentral surface of about  $40x80 \text{ km}^2$ , with the depth of the foci between 60 and 170 km.

The most powerful earthquake produced by this source is considered to be that of October 26, 1802, having a magnitude of 7.9.

In the 20th century, on November 10, 1940, the earthquake with the highest magnitude of the century (magnitude 7.7) occurred at a depth of 140-150 km, and on March 4, 1977 it was recorded the first accelerogram of a strong earthquake. Being the earthquake with the most destructive effect of the twentieth century, the seismic event of `77 recorded a magnitude of 7.4, with a focal depth of 94 km and an average epicentral distance from Bucharest of 130 km. In the predominantly clayey site conditions of the INCERC site, in the east of Bucharest, a maximum ground acceleration of 0.2g was recorded, with a predominant period of very long ground vibration, of 1.45s.

On August 30, 1986, a 7.1 magnitude earthquake occurred at a focal depth of 133 km. It registered in the epicentral area, in Focșani, a maximum acceleration of 0.3g, and in the north of Bucharest (in the Free Press Square) a maximum acceleration of the land of 0.16g.

On May 30, 1990, an earthquake of magnitude 6.9 on and depth of 91 km recorded peak accelerations in Bucharest between 0.07g and 0.13g.

According to the catalog of earthquakes Romplus INFP (Radulian et al., 2009) from the beginning of the twentieth century until now, there have been 14 earthquakes with magnitude greater than 6.3, the largest being that of November 10, 1940, but only 4 of these earthquakes were recorded. Earthquakes with magnitude less than 6.3 are considered insignificant for the calculation of constructions.

The seismic design code P100-1/2013 (MDRAP, 2014) offers the possibility to design using the dynamic calculation method with the input of real, artificial or simulated accelerograms, but respecting certain restrictions regarding the number of accelerograms used, their compatibility with the seismic hazard of the area, the scaling factors and others. These restrictions determine the need for artificial or simulated accelerograms. Of these, artificial accelerograms are made on the basis of elastic response spectra (although widely used because they mimic response spectrum are generally unrealistic because they do not reproduce the non-stationarity of the natural seismic motion - Pavic et al., 2000). The

simulated ones are realized starting from the characteristics of the seismic source mechanism, the influence of the seismic wave path and the influence of the local site conditions. Thus, the use of simulated accelerograms in the design of new buildings or the consolidation of existing ones is the method that captures the characteristics of the natural phenomenon in a greater complexity, which implies a deeper knowledge of the hazard, and this reduces the risk.

Currently, there are four main methods for predicting seismic motion: ground motion prediction equations (the result of the method being motion parameters), stochastic modeling, empirical Green functions and numerical modeling based on physical characteristics (the last three methods resulting in time domain motion). In recent years, hybrid methods that combine numerical modeling, empirical Green functions and stochastic modeling have been used. The difficulty of the earthquake simulation methods is given by the complexity of the input data. While for the ground motion prediction equations it is necessary to identify the general characteristics of the seismic source, the fault geometry, the definition of the rupture (seismic moment, tectonic mechanism, the slip type), for the stochastic method it is necessary to characterize the influence of the propagation path in terms of seismic wave velocities and densities and local behavior of the ground near the free surface. Numerical modeling also requires more input data: a proper characterization of the seismic source (kinematic or dynamic) and a more detailed definition of the geological complex that can influence the local seismic response.

Some examples of simulation methods are:

Beresney, I. A. and Atkinson, G. M. (1998). FINSIM — A FORTRAN Program for Simulating Stochastic Acceleration Time Histories from Finite Faults. Seismol. Res. Lett., 69:27–32.

Boore DM (2005) SMSIM—Fortran programs for simulating ground motions from earthquakes: version 2.3—a revision of OFR 96-80-A. U.S. Geological Survey Report OFR 00–509

Furumura, T., Hayakawa, T., Nakamura, M., Koketsu, K., and Baba, T. (2006). Development of Long-Period Ground Motions from Earthquakes Within the Nankai Trough, Japan: Observations and Computer Simulation of the 1944 Tonankai (Mw 8.1) and 2004 SE Off-Kii Peninsula (Mw 7.4) Earthquakes. Pure Appl. Geophys., submitted.

Furumura, T., Koketsu, K., and Wen, K.-L. (2002). Parallel PSM/FDMHybrid Simulation of Ground Motions from the 1999 Chi-Chi, Taiwan, Earthquake. Pure Appl. Geophys., 159:2133–2146.

Kamae, K., Irikura, K., and Pitarka, A. (1998). A Technique for Simulating Strong Ground Motion Using Hybrid Green's Function. Bull. Seismol. Soc. Am., 88:357–367.

Miyake, H., Iwata, T., and Irikura, K. (2003). Source Characterization for Broadband Ground-Motion Simulations: Kinematic Heterogeneous Source Model and Strong Motion Generation Area. Bull. Seismol. Soc. Am., 93:2531–2545.

Suzuki, W., Iwata, T., Asano, K., and Yamada, N. (2005). Estimation of the Source Model fort he Foreshock of the 2004 off the Kii Peninsula Earthquakes and Strong Motion Simulation of the Hypothetical Tonankai Earthquake Using the Empirical Green's Function Method. Earth Planets Space, 57:345–350.

#### 2. Empirical Green's function method

The method involves modeling a large earthquake (large rupture surface) through a series of small earthquakes that represent point sources along a fault (with a focal mechanism similar to the target earthquake), taking into account the propagation of the rupture through phases of delay. Basic works in the literature on the empirical Green's functions are Hartzell (1978), Kanamori (1979), Irikura (1983, 1986), Miyake (2003).

Hartzell (1978) associates the response of each point source with the movement of the nearest associated aftershock (which becomes a Green function), so the effect of the ground's structure is surprised and the source mechanism is no longer needed.

The empirical Green's function method formulated by Irikura (1986) is based on the law of scaling the parameters of the fault for large and small events of Kanamori and Anderson (1975) and the omega square spectral source defined by Aki (1967). The shape of the seismic waves of a large event is synthesized by summing small recorded events corrected for the differences in rupture velocity.

The summation of small events is performed by the following equations:

$$\begin{split} U(t) &= \sum_{i=1}^{N} \sum_{j=1}^{N} \frac{r}{r_{ij}} F(t) * \left( C \cdot u(t) \right) \\ F(t) &= \mathcal{S}(t - t_{ij}) + \frac{1}{n'} \sum_{k=1}^{(N-1)n'} \left[ \mathcal{S}\{t - t_{ij} - \frac{(k-1)T}{(N-1)n'}\} \right] \end{split}$$

$$t_{ij} = \frac{r_{ij} - r_o}{V_s} + \frac{\xi_{ij}}{V_r}$$

where

U(t) is the simulation of the seismic waves of the big event, u(t) the small event, N and C are fractions of the dimensions of the fault and the stress drop taking into account the differences between the major event and the small events.

F(t) is the correction function that adjusts the differences between breaking functions between small and large events

 $V_s$  and  $V_r$  are the velocities near the source and the rupture velocity

T is the risetime

n` is is an integer that weakens the artificial periodicity given by n.

Through the 1997 paper, Irikura et al. proposed to change the function F(t):

$$F(t) = \mathcal{S}(t-t_{ij}) + \frac{1}{n'(1-\frac{1}{e})} \sum_{k=1}^{(N-1)n'} \big[ \frac{1}{e^{\frac{(k-1)}{(N-1)n'}}} \mathcal{S}\{t-t_{ij} - \frac{(k-1)T}{(N-1)n'}\} \big]$$

The values of N and C are determined from the equations:

$$\frac{U_o}{u_o} = \frac{M_o}{m_o} = CN^3$$

$$\frac{A_o}{a_o} = CN$$

where  $U_0$  and  $u_0$  are the spectral amplitudes of the big event, respectively of the small event,  $M_0$  and  $m_0$  are the seismic moments of the events,  $A_0$  and  $a_0$  are the levels of constant spectral amplitude of the events.

After solving the system of equations it results:

$$N = \left(\frac{U_0}{u_0}\right)^{\frac{1}{2}} \left(\frac{a_0}{A_0}\right)^{\frac{1}{2}}$$

$$C = \left(\frac{u_0}{U_0}\right)^{\frac{1}{2}} \left(\frac{A_0}{a_0}\right)^{\frac{3}{2}}$$

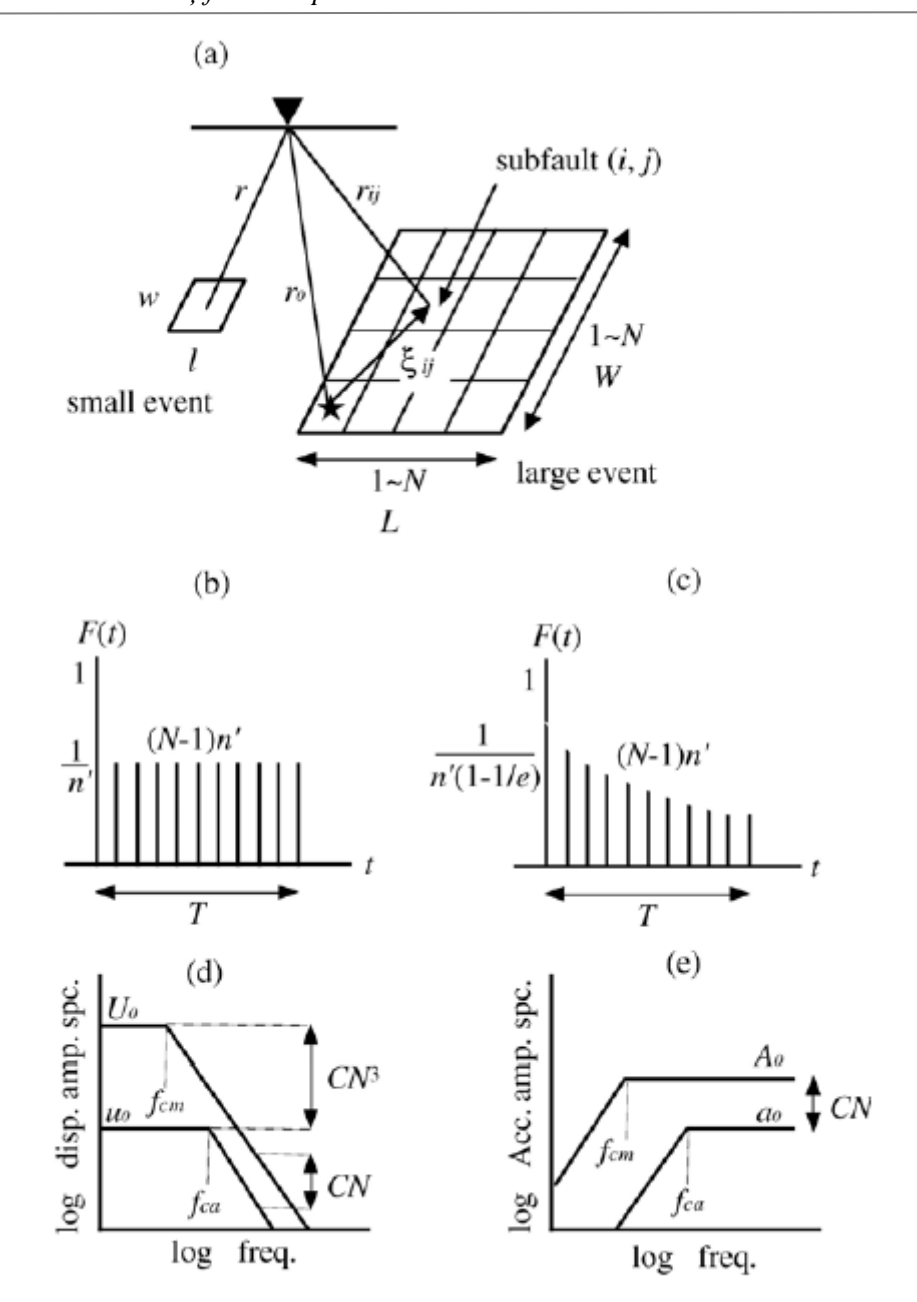


Figure 1 Schematic illustration of the Green's empirical function method. (a) Fault areas (small and large). (b) Filter to adjust to the difference in slip velocity function between the large and small events according to Irikura 1986 (the function is a sum between a delta and boxcar function). (c) Filter modified according to Irikura et al. 1997 with an exponential function instead of a boxcar function where T is the risetime for the large event. (d) Schematic displacement amplitude spectra following the omega-squared source scaling model, assuming a stress drop ratio C between the large and small events. (e) Acceleration amplitude spectra following the omega-squared source scaling model (Lecture Note on Strong Motion Seismology, K. Irikura and H. Miyake)

#### 3. Stochastic simulations

Hanks and McGuire (1980) demonstrate that high-frequency accelerations can be described as limited-band Gaussian noise with certain spectral characteristics. It can also be assumed that the acceleration phase of the seismic motion is random. Thus, they combined spectral models of the seismic motion with the notion that, in practice, high frequency motions are random (HANKS, 1979; McGuire and HANKS, 1980; and McGuire, 1981). In the work of Hanks and McGuire (1980), they assumed that the accelerations on an elastic semi-space are of limited band, of finite duration, of white or of Gaussian noise type, and that the source spectrum is described by a single-corner frequency model, depending on the size of the earthquake, and they derived a simple relationship that describes the peak acceleration of a earthquake.

Boore (1983) generalized their work to allow the use of more complex, extended models to simulate time series and to allow more features of seismic motion to be considered. The equation of the spectrum of the seismic motion used by Boore (2003) is as follows:

$$Y(MO,R,F) = E(M_0,f)P(R,f)G(f)I(f)$$
, where:

 $M_0$  – is the seismic moment (Aki, 1966), the transformation between the seismic moment and the moment magnitude being given by the relationship (Hanks and Kanamori, 1979):

$$M_w = \frac{2}{3} \log M_0 - 10.7,$$

and the transformation of the Gutenberg-Richter magnitude into moment magnitude is performed according to Lungu et al. (2003) with the following relationship:

$$M_W \cong M_{GR} + 0.3$$

E – function that describes the focar mechanism;

P – function describing the influence of wave propagation media;

G – function describing the influence of local site conditions;

I – function that takes into account the type of motion.

In the specialized literature we find, for modeling the seismic source, two popular methods: point source stochastic modeling and finite source stochastic modeling. Also, the source spectrum can be defined as having one or two corner frequencies. In the following, the principles of each type of modeling will be presented briefly.

#### a. Point source stochastic modeling

The point source stochastic model assumes that the source is concentrated in a point and that the generated time series accelerations, at a given location, take into account both deterministic and random characteristics of the seismic motion. The deterministic characteristics are specified through the average of the Fourier spectrum, by a function of magnitude and distance. The stochastic characteristics are generated by modeling the seismic motion as a noise with certain spectral characteristics.

This type of modeling is advantageous if the source to surface distance is greater than the source dimensions (Boore, 1983, 2003; Boore and Atkinson, 1987; Atkinson and Boore, 1995, 1997; Atkinson and Silva, 1997, 2000).

The steps of performing a stochastic simulation using point source modeling are as follows:

- the noise (Gaussian or white) is generated for a duration given by the duration of the motion;
- the noise is then windowed;
- the windowed noise is transformed into the frequency domain;
- the spectrum is normalized by the square-root of the mean square amplitude spectrum;
- the normalized spectrum is multiplied by the ground motion spectrum Y;
- the resulting spectrum is transformed back to the time domain.

b. Finite source stochastic modeling

To take into account the effects that the point source modeling cannot surprise, Hartzell (1978) proposes dividing the surface of the fault into a grid of subfaults and treating each one as a Brune type point source, with a single corner frequency spectrum.

The rupture mechanism is described through the following steps:

- randomly choosing a subfault from which the rupture starts (hypocenter),
- the rupture propagates in all directions along the fault,
- a subfault is triggered when the propagation of the rupture reaches its center,
- the simulations from an observation point are generated by summing the time series of the subfalts, offseted in time taking into account the delays caused by the propagation of the rapture,
- calculation of Fourier spectra for simulated recordings at several azimuths, located at observation points located equidistantly around the fault
- defining the shape and amplitude levels of an equivalent point-source spectrum that mimics the effects of the finite phase using the average Fourier spectrum.

\_

12

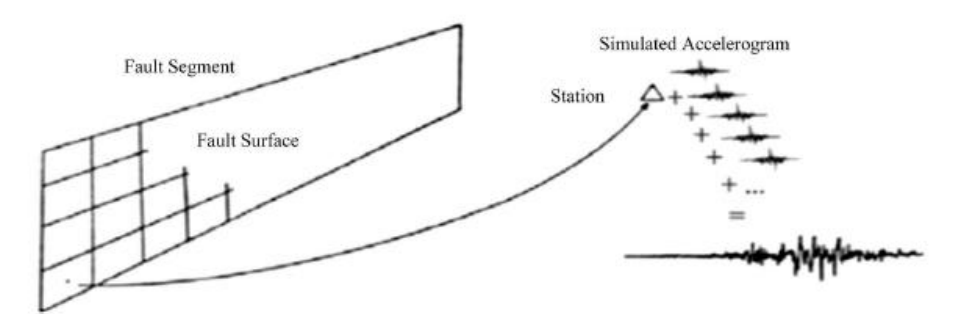


Figure 2. The principle of obtaining the simulated accelerograms using the finite source model (Boore 2003)

#### c. Single corner frequency source spectrum

The simplest and most common model for modeling the source spectrum is the  $\omega^2$  model with a single corner frequency (Brune, 1970, 1971). Ignoring the multiplicative constants, the Fourier spectrum of accelerations (FAS) has the following formula:

$$S_a(M_0, f) \propto \frac{M_0 f^2}{1 + (f/f_c)^2}$$

where  $M_0$  is the seismic moment, and  $f_0$  is the corner frequency.

The spectrum of the source accelerations is flat for the frequency grater than the corner frequency; for high frequencies its value is given by the relation:

$$S_{aHF}(M_0,f) \propto M_0 f_c^2$$

In this model the corner frequency depends on the seismic moment  $M_0$ , the stress drop  $\Delta \sigma$  and the shear wave velocity  $\beta s$ .

$$f_0 = 4.9 \times 10^6 \beta_s (\frac{\Delta \sigma}{M_0})^{1/3}$$

#### d. Double corner frequency source spectrum

After analyzing sets of records Atkinson and Boore (1995) developed a new model for the source spectrum, a double frequency model. It has been shown that it better captures the spectral characteristics of the sources (than the single-corner model). For the double frequency model there are several methods for defining the spectral form: Atkinson and Boore (1995), Haddon (1996), Joyner (1997) and Atkinson and Silva (2000). The shape of the source spectrum depends on the two corner frequencies,  $f_a$  and  $f_b$ , and these depend on the seismic moment. The models with double corner frequency are multiplicative or additive, and in the table presented below the different models with the corresponding formulas for the Fourier spectrum of accelerations of the source are illustrated:

$$S(M_0,f) = Sa(M_0,f) \times Sb(M_0,f)$$

Model <sup>†</sup>	$S_a$	$S_b$
BC92	$f < f_a : 1$ $f \ge f_a : f_a/f$	$\frac{1}{(1+(f/f_b)^2)^{1/2}}$
AB95 Fea96*	$\frac{J \ge Ja \cdot Ja/J}{\frac{1-\epsilon}{1+(f/f_a)^2} + \frac{\epsilon}{1+(f/f_b)^2}}$ $\frac{1-\epsilon}{1+(f/f_a)^2}$	1 1
H96	$\frac{1}{(1+(f/f_a)^8)^{1/8}}$	$\frac{1}{(1+(f/f_b)^8)^{1/8}}$
J97	$\frac{1}{(1+(f/f_a)^2)^{3/4}}$	$\frac{1}{(1+(f/f_b)^2)^{1/4}}$
AS00	$\frac{1-\epsilon}{1+(f/f_a)^2} + \frac{\epsilon}{1+(f/f_b)^2}$	1

Table 1 Spectrum types for source definition (Boore, 2003)

The common characteristics of these models are given by the fact that for low frequencies the amplitude increases proportionally with the seismic moment, and for high frequencies the spectrum becomes flat, with an amplitude equal to that of the single-corner model.

The effect of seismic wave propagation media is quite complicated due to the wave propagation angles and their reflection, but for most applications, it is recommended to represent the effects of propagation media by simple functions, which include the geometrical spread of waves, attenuation (obtained by combining intrinsic attenuation and scatter attenuation) and the overall increase of duration with the distance, as a result of wave propagation and scattering.

The simplified effect of propagating media is given by the following equation:

$$P(R, f) = Z(R)e^{\left[-\pi f R/Q(f)c_Q\right]}$$
, where

Z(R) – the geometrical spreading function given by the following equation:

$$Z(R) = \begin{cases} \frac{R_0}{R} & R \le R_1 \\ Z(R_1)(R_1|R)^{p_1} & R \le R_2 \\ \vdots & & \\ Z(R_n)(R_n|R)^{p_n} & R_n \le R \end{cases}$$

R – the hypocentral distance, but in applications it is taken as the closest distance to the rupture surface. In certain applications it is necessary to include, depending on the source modeling, the influence of the "pseudo-depth" h, determined empirically. According to Boore et al. (1997)  $R = \sqrt{D^2 + h^2}$ , where D is the closest distance to the vertical projection of the surface of the rupture on the surface. The figure below shows the geometrical spreading in a prediction model of the seismic motion used by Atkinson and Boore (1995).

Q(f) – seismic attenuation, this is determined by analyzing a database;

14

 $c_Q$  - seismic velocity used to determine attenuation Q(f).

Basically, the effects of local site conditions would be included in the path effects, but because the local site effects are independent of the traveled distance from the source (if nonlinear effects are not taken into account) is indicated to separate them from the path effects. Separating the amplification effect A(f) from the attenuation effect D(f), the equation of local location effects is as follows:

$$G(f) = A(f)D(f)$$

The amplification function A(f) is usually in relation to the source. The diminution function D(f) is used to model the energy loss independent from the path (the path dependent part is expressed by the exponential term in the equation of influence of propagation media). The effect of nonlinearity is not taken into account in this method.

Amplification A(f) can be calculated either by a calculation that takes into account the reflection of the waves, or by a calculation assuming that the amplification of the waves is given by the square root of the ratio between the source impedance and the surface impedance:

$$A(f(z)) = \sqrt{Z_s/\bar{Z}(f)}$$

 $Z_s = \rho_s \beta_s$  - the seismic impedance near the source, where  $\rho s$ ,  $\beta s$  are the density, respectively the velocity of the seismic waves near the source;

$$\bar{Z}(f) = \int_{0}^{t(z(f))} \rho(z)\beta(z)dt / \int_{0}^{t(z(f))} dt$$

- the average of the seismic impedance near the surface;

t(z(f)) – the time when the shear waves reach from the depth z(f) to the surface;

$$f(z) = 1 / \left[ 4 \int_{0}^{z(f)} \frac{1}{\beta(z)} dz \right]$$

- depth is a function of frequency and is chosen such that z is a quarter of the wavelength of the seismic waves at average velocity  $\bar{\beta}=z(f)/\int_0^{z(f)} [1/\beta(z)]dz$ 

In practice, it is easier to use the seismic impedance near the surface as a function of depth:

$$\bar{Z}(f) = \int_{0}^{z(f)} \rho(z) dz / \int_{0}^{z(f)} \frac{1}{\beta(z)} dt$$

simplified  $\bar{Z}(f) = \bar{\rho}\bar{\beta}$ , where

$$\bar{\rho} = \frac{1}{z(f)} \int_{0}^{z(f)} \rho(z) dz$$

$$\bar{\beta} = z(f) \left[ \int_{0}^{z(f)} \frac{1}{\beta(z)} dz \right]^{-1}$$

The attenuation D(f) represents the path independent loss of the high frequency motion. This loss may be due to a source effect (Papageorgiou and Aki 1983B), a local site effects (Hanks 1982) or a combination of these effects. Thus for modeling the effects, two filters (which can be used separately or in combination) can be used:

- filter  $f_{max}$  (Hans 1982, Boore 1983)

$$D(f) = [1 + (f/f_{max})^8]^{-1/2}$$

- filter k<sub>0</sub> (Anderson și Hough 1984)

$$D(f) = \exp(-\pi k_0 f)$$

An example of a combined effect is shown in the figure below (Boore and Joyner, 1997):

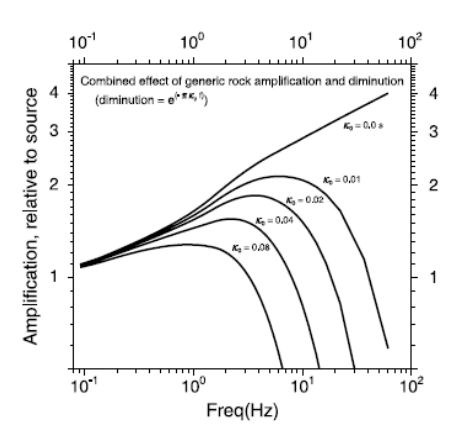


Figure 3. The combined effect of the site (taking into account both amplification and diminution) (Boore 2003)

#### 4. Physical based numerical modeling. Theoretical simulations (3D)

The most appropriate method for simulating long-period seismic motion is the method of the fourth-order finite difference with spatial grid variables (Pitarka 1999) and frequency-dependent attenuation factor [Irikura and Miyake, Lecture Note]. This method involves building a 3D velocity model and determining the optimal attenuation parameter, the resulting waves being 3D.

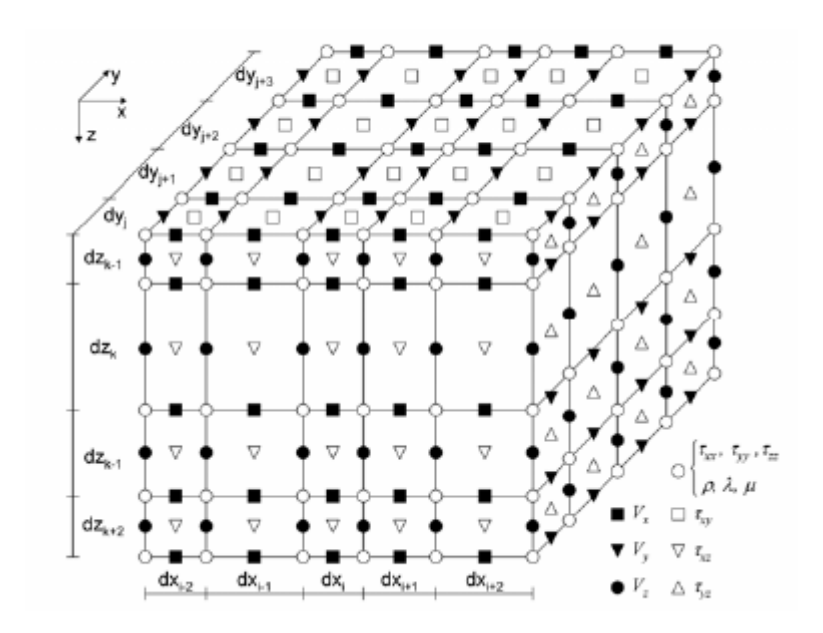


Figure 4. Example of spatial grid used in simulations with numerical methods (Irikura and Miyake, Lecture Notes)

The following set of equations describes the propagation of 3D waves in a linearelastic isotropic environment:

Moment preserving equations:

$$\begin{split} \rho \partial_{tt} u_x &= \partial_x \tau_{xx} + \partial_y \tau_{xy} + \partial_z \tau_{xz} + f_x \,, \\ \rho \partial_{tt} u_y &= \partial_x \tau_{xy} + \partial_y \tau_{yy} + \partial_z \tau_{yz} + f_y \,, \\ \rho \partial_{tt} u_z &= \partial_x \tau_{xz} + \partial_y \tau_{yz} + \partial_z \tau_{zz} + f_z \,. \end{split}$$

Effort-deformation relationships:

$$\begin{split} &\tau_{xx} = (\lambda + 2\mu)\partial_x u_x + \lambda(\partial_y u_y + \partial_z u_z)\,,\\ &\tau_{yy} = (\lambda + 2\mu)\partial_y u_y + \lambda(\partial_x u_x + \partial_z u_z)\,,\\ &\tau_{zz} = (\lambda + 2\mu)\partial_z u_z + \lambda(\partial_x u_x + \partial_y u_y)\,,\\ &\tau_{zz} = \mu(\partial_y u_x + \partial_x u_y)\,,\\ &\tau_{xz} = \mu(\partial_z u_x + \partial_x u_z)\,,\\ &\tau_{yz} = \mu(\partial_z u_y + \partial_y u_z)\,. \end{split}$$

#### 5. Hybrid methods

The simulation of the seismic motion produced by a large event near the source has a good accuracy if there is a detailed knowledge about the distribution of the slip along the fault and about the geological structure crossed by wave from source to surface. Hybrid simulation methods combine long-period movements of a large earthquake (simulated by deterministic methods) and short-period movements (simulated using either stochastic methods suitable for small earthquakes or using empirical Green functions suitable for large earthquakes). Simulated ground motion results from the summation of long-period movements and short-period movements after filtering.

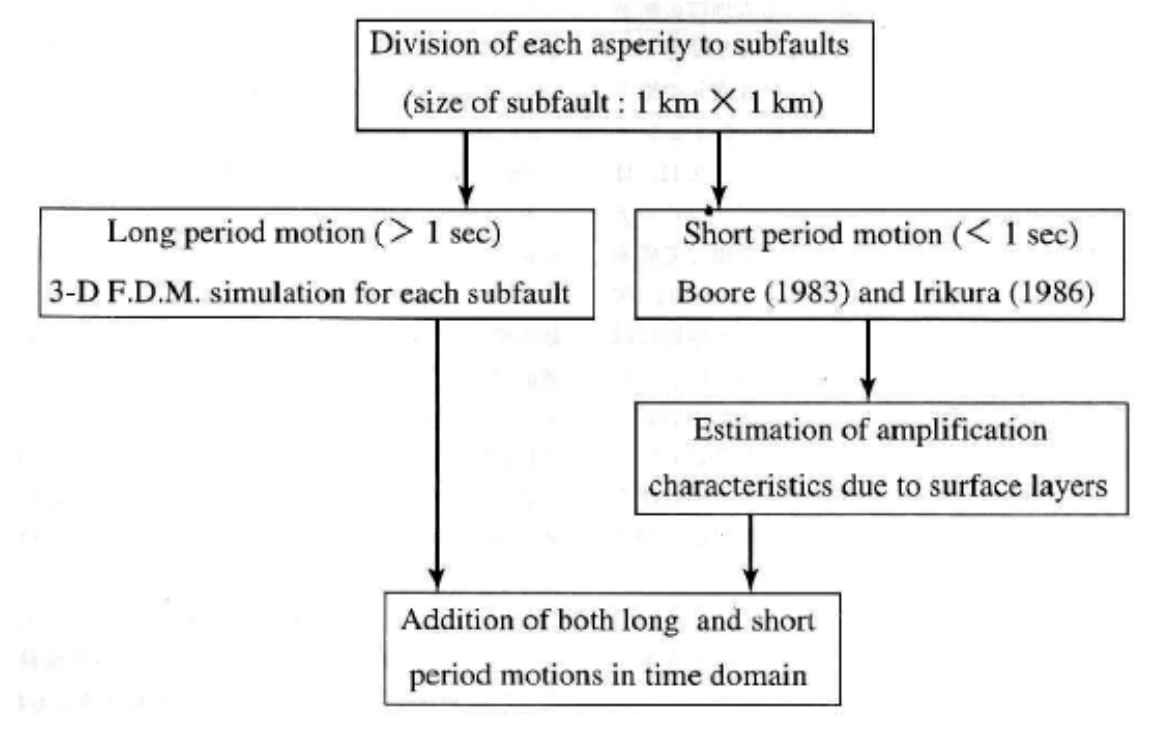


Figure 5. Hybrid seismic motion simulation method for large earthquakes (Irikura and Miyake, Lecture Notes)

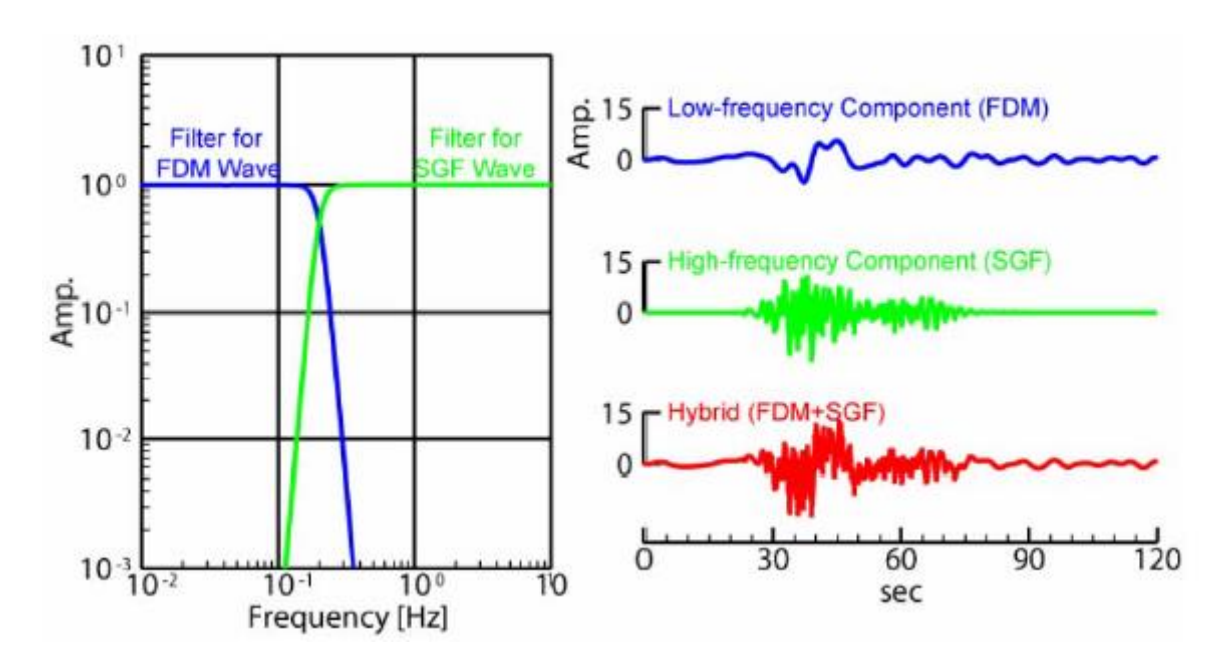


Figure 6. Examples of filters used in hybrid method and example of large earthquake simulation (Morikawa et al., 2006)

## 6. Simulations of the ground motion generated by the intermediate depth earthquake in October 27, 2004 at INCERC station. Interpretation of results

#### **6.1.** Earthquake characteristics

The Vrancea seismic source is characterized by a reverse faulting rupture (Radulian et.al., 2000). The vrancean source has a small volume and intermediate depth, these characteristics being given that the radii from all the hypocenters to a station are approximately equal and the smallest hypocentral distance is 90 km. Another property of the foci is the lateral inhomogeneity of the source due to its geometry.

The earthquake of October 27, 2004 belongs to the category of medium earthquakes with a magnitude of 5.8 at a focal depth of 99km (according to Oth et al. 2007) or 105km (according to Vacareanu et al. 2014). The epicenter of this earthquake is at 45.78° latitude N and 26.73° longitude E (according to Oth et al. 2007) or 45.78° latitude N and 26.73° longitude E (according to Vacareanu et al. 2014). The dimension of the seismic fault according to Oth et al. 2007 was 1.2x 1.8km, and the stress drop was 75bari (according to Ganas et al. 2010). From the point of view of the focal mechanism according to Ganas et al. 2010 the earthquake was produced at a strike of 219°, the dip being 81°, with a rake of 107°.

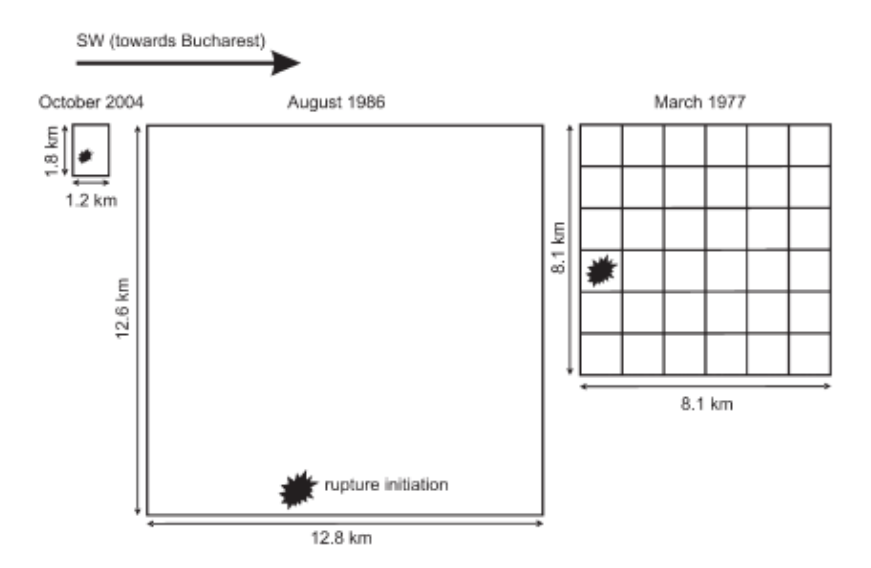


Figure 7. The faults dimensions of the earthquake October 27, 2004, August 30, 1986, and March 4, 1977 (Oth et al., 2007)

Simulations were performed for the Vrancean subcrustal earthquake on October 27, 2004 using the SMSIM program made by Boore (2005).

#### **6.2.** The first set of simulations

#### **Input data**

For the average velocity of the shear waves  $\beta s$  and the density  $\rho$  near the source, in the literature, several variants are used, so Martin et al. (2006) propose  $\beta s = 4.5$  km/s and denistivity  $\rho = 3.2$  g/cm<sup>3</sup>, and Sokolov (2008) proposes  $\beta s = 3.8$  km/s and denistivity  $\rho = 2.8$  g/cm<sup>3</sup>. In the simulation, the average velocity of shear waves  $\beta s = 4.5$  km/s was considered, and the density  $\rho = 2.8$  g/cm<sup>3</sup>.

For the constant  $C = \langle R_{\Theta\Phi} \rangle VF / (4\pi \rho_s \beta_s^3 R_0)$ , the considered values are:

 $\langle R_{\theta\phi} \rangle$  – the average radiation pattern is 0.6 according to Oth et al. (2008)

V - the horizontal component of the total energy of the shear waves given by the two-way decomposition (=  $1/\sqrt{2}$ );

F - the effect of the free surface is 2;

 $R_0$  - the reference distance is 1 km.

From the source point of view, simulations were performed for 3 types of spectra for the source: the source with a single corner frequency (S1) and with two corner frequencies with additive (S11) and multiplicative spectrum (S12). The used models are (according to Table 1) BC92 for Source 1 (Boatwright and Choy 1992), H96 for Source 11 (Haddon 1996)

and AB95 for source 12 (Atkinson and Boore 1995). The corner frequency being defined according to Gusev et al. (2002):  $Mw = -2\log(fc) + 4.84$ .

For the calculation of scattering and attenuation Pavel and Vacareanu (2015) modeled by regression the Fourier amplitude spectra from the locations where the soil conditions were of class B or C (according to EN 1998-1: 2004). For earthquakes with magnitudes greater than 6.9 they observed good scattering fit, for long and medium frequencies, for  $1/R^{0.5}$ , where  $R = \sqrt{D^2 + h^2}$ . So Z(R) – the scatter function is given by the following equation:

$$Z(R) = (1|R)^{0.5}$$

For the hypocentral distance, two sets of simulations were performed, one for where D = 154 km (the epicentral distance to Bucharest), h = 99 km, that is R = 183 km and another for Reff = 188 km the effective distance taking into account the fault geometry (calculated using the reff.exe executable from the SMSIM program set). The effective distance results from solving the equation:

$$G(R_{\text{EFF}}) \exp(-\pi f_{Q} R_{\text{EFF}}/Q(f_{Q}) V_{S}) = \left[ \frac{1}{N} \sum_{i=1}^{N} \{ G(R_{i}) \exp(-\pi f R_{i}/Q(f) V_{S}) \}^{2} \right]^{1/2}$$

where G(R) is the geometrical scattering,  $R_i$  is the hypocentral distance of each subfault, Q(f) is the attenuation,  $f_Q$  is the reference frequency (usually 10Hz), and Vs the velocity of the seismic shear waves. According to Boore 2009, the use of the effective distance in the simulations performed in SMSIM (stochastic simulation program for point sources made by Boore) takes into account the geometry of the fault and the results are close to those given by EXSIM (program of stochastic simulation for finite fault type sources made by Motazedian and Atakinson 2005) if a 50% pulsed source is used.

Benetatos et al. (2003) defines the geometric scattering as 1/R for R < 100 km and  $1/R^{0.5}$  for R > 100 km, the reference distance being  $R_0 = 1 \text{km}$ , and 0th et al. (2008) defines it as  $R_0/R$ , the reference distance being  $R_0 = 90 \text{km}$ . In these sets of simulations the geometric scattering was considered according to Pavel and Vacareanu (2015).

Regarding the attenuation, in the same work previously mentioned Pavel and Vacareanu (2015) determined it as having the form  $Q(f) = 100xf^{1.20}$  (form used in the performed simulation). Following the analysis of the seismic wave attenuation, Oth (2007) found the form of the attenuation equation being  $Q(f) = 100 x f^{0.80}$ , Mândrescu et al. (1993) defines it as  $Q(f) = 109 x f^{0.81}$ , and in Pavel (2015) it can be found as  $Q(f) = 165 x f^{1.20}$ .

A significant dependence of the earthquake magnitude parameter and local site was observed (Radulian et al. 2000). For example, for the Bucharest area, the mean value  $k_0$  has a relatively high value of 0.071, in the area of Moldova the average value  $k_0$  is 0.057 and in the epicentral area  $k_0$  has an average value of 0.101. For the application, the values of the kappa parameter were considered in the work of Pavel and Vacareanu (2015). The kappa spectral degradation parameter was calculated using the recordings of the nine earthquakes recorded

by 57 seismic stations. The final value of the kappa parameter is given by the following equation  $k = k_{event} + k_0$ , where  $k_{event} = 0.022 M_w - 0.127$ . Another study, conducted by Sokolov et al. (2008), provides a relation for the kappa parameter of the form  $k = 0.01 M_w$ . Thus, for the application of this paper k = 0.074.

The duration of the sources was considered according to Boore (2003), and the path dependent duration was considered 0.0868 used in the paper of Pavel (2016). For amplification of the location site conditions, two amplification profiles were used, one resulting from the calculation performed with the NRATTLE (program from the SMSIM collection) for the shear wave profile for INCERC Bucharest (Constantinescu and Enescu, 1985), the second is an amplification profile used in the paper of Pavel (2016) resulting from the H/V method.

#### **Modified parameter (calibration)**

Starting from the assumption that in the simulations performed by Boore (2003), Pavel and Vacareanu (2015), Oth et al. (2007), Sokolov et al. (2008) the stress drop parameter was chosen higher than could be found in the specialized parameters (for example for the 1977, 1986 earthquakes - Ganas et al. 2010, Oncescu and Bonjer 1997). The stress drop parameter was changed from 75 bars to 300 bars, and 4 sets of 400 simulations were performed for Source 1, the H/V amplification profile. An arithmetic mean of the simulation type peak acceleration ranging from 17.97 cm/s² to 41.92 cm/s² was obtained according to the table below.

Type of simulation using	Arithmetic	Geometric
SMSIM	mean	mean
SIVISHVI	$(cm/s^2)$	$(cm/s^2)$
04sursa1RH_V75stress	17.97	17.79
04sursa1RH_V200stress	29.96	29.69
04sursa1RH_V250stress	37.27	36.90
04sursa1RH_V300stress	41.49	41.10

Table 2 Average peak acceleration for different stress values

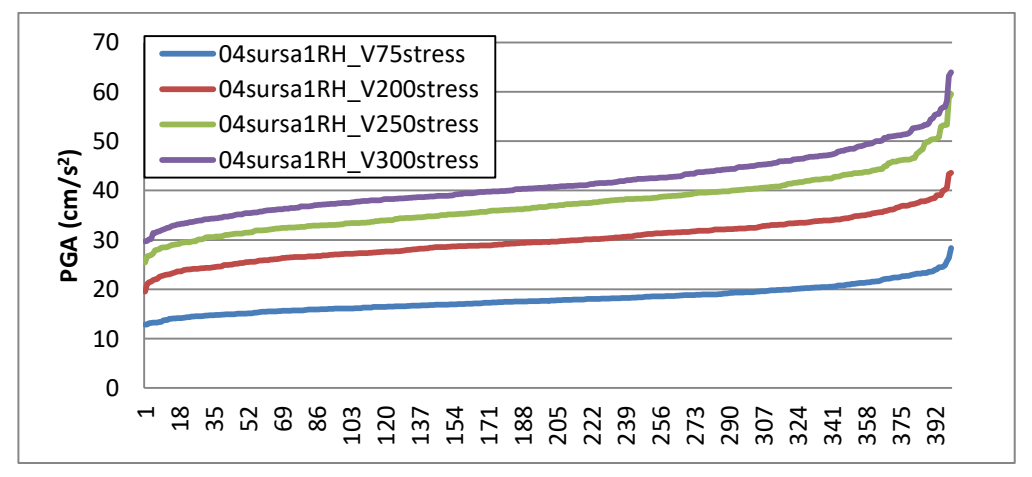


Figure 8. Variation of peak accelerations within the sets of 400 simulations for each of the 4 values of stress drop

#### **Interpretation of results**

By setting the stress parameter at 200 bars, simulations were performed for the 3 source types, two source-station distances (a geometrical one of 183 km, and an effective one of 188 km which takes into account the geometry of the fault). For the source S1, two types of amplifications of local site conditions were used (NRATTLE results and H/V profile).

From the 400 simulation sets, an accelerogram with the closest PGA value to the average was analyzed.

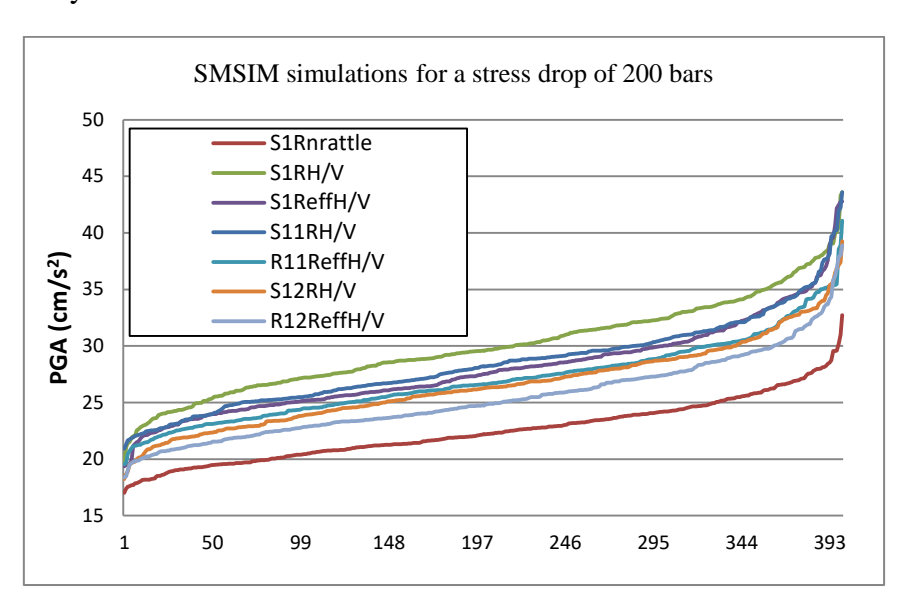


Figure 9. Variation of peak accelerations in the 400 simulations performed for the three source types and 2 local amplification types (the PAGs values were ordinated for a better illustration of the differences)

Type of simulation using SMSIM	Effective duration	Average square root	PGA (cm/s <sup>2</sup> )	Source duration	Path duration	Total duration	fa (Hz)	fb (Hz)	Obs.
Vrancea 2004 NS	21.39	3.8	30.01				0.35	0.35	*f <sub>0</sub> cf.
Vrancea 2004 EW	20.92	3.4	29.72				0.35	0.35	Gusev et al 2002
Sursa1 R H/V	16.73	7.8	30.65	1.37	15.8	17.26	0.726	0.726	
Sursa1 Reff H/V	17.1	8.1	28.36	1.37	16.31	17.69	0.726	0.726	fa=fb=f0
Sursa1 R nrattle	15.93	5.9	22.59	1.37	15.88	17.26	0.726	0.726	
Sursa11 R H/V	15.89	8.3	28.75	2.22	15.88	18.11	0.25	2.09	
Sursa11 Reff H/V	15.79	8.7	27.1	2.22	16.31	18.54	0.25	2.09	
Sursa12 R H/V	16	7.9	26.93	1.32	15.88	17.21	0.5	1.52	
Sursa12 Reff H/V	14	7.4	25.42	1.32	16.31	17.64	0.5	1.5	

Table 3. Characteristics of simulated ground motion of October 27, 2004 for a 200 bar stress drop

#### Conclusions:

1. From the point of view of amplification given by local conditions, one can notice a decrease of peak accelerations about 1.35 times between the H/V and NRATTLE amplification profile.

- 2. Using the reference distance leads to a decrease in peak accelerations on average by 2.3 cm/s<sup>2</sup> for Source 1 and by 1.6 cm/s<sup>2</sup> for Sources 11 and 12 compared to the simulations in which the closest distance was used.
- 3. The significant duration of the earthquake recorded in 2004 is on average about 4 seconds longer than the simulations duration.
- 4. It can be seen that the mean square acceleration (parameter measuring the effects of amplitude and frequency content) is about 2.2 times higher for the simulations made using the H/V amplification profile, and for the simulation performed with the NRATTLE amplification profile is about 1.6 times higher (the difference can be explained by the large difference between peak accelerations).
- 5. Seismic energy is released faster and more abruptly through simulated ground motions than real accelerograms.
- 6. It can be noticed that all simulations fail to capture the 2004's earthquake peaks for periods of less than 0.25 s (frequencies higher than 4 Hz).
- 7. Simulations in which the reference distance was used tend to capture a peak for periods of 0.20s (S1) -0.3s (S11, S12). Also, for two-frequency corner sources at longer periods, amplification has a closer reduction to reality.

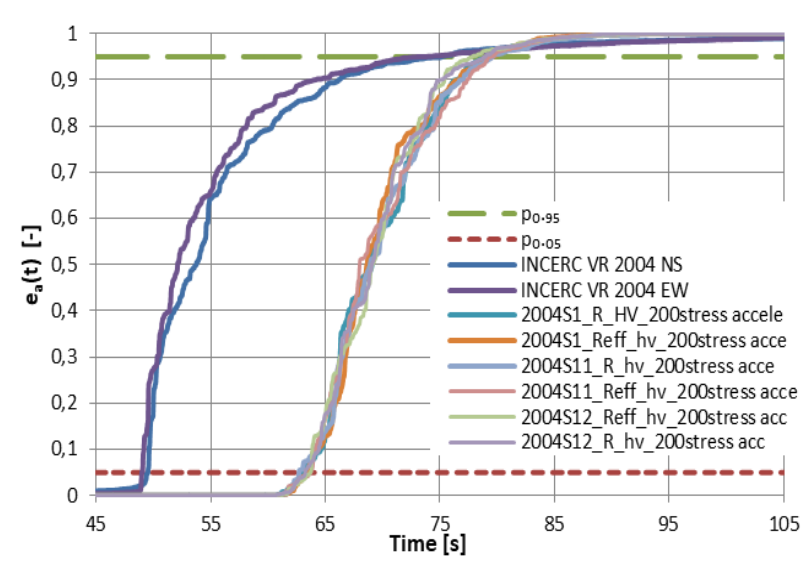


Figure 10. Cumulative energies of actual records and simulations with SMSIM Energiile cumulative ale simulărilor și înregistrărilor reale

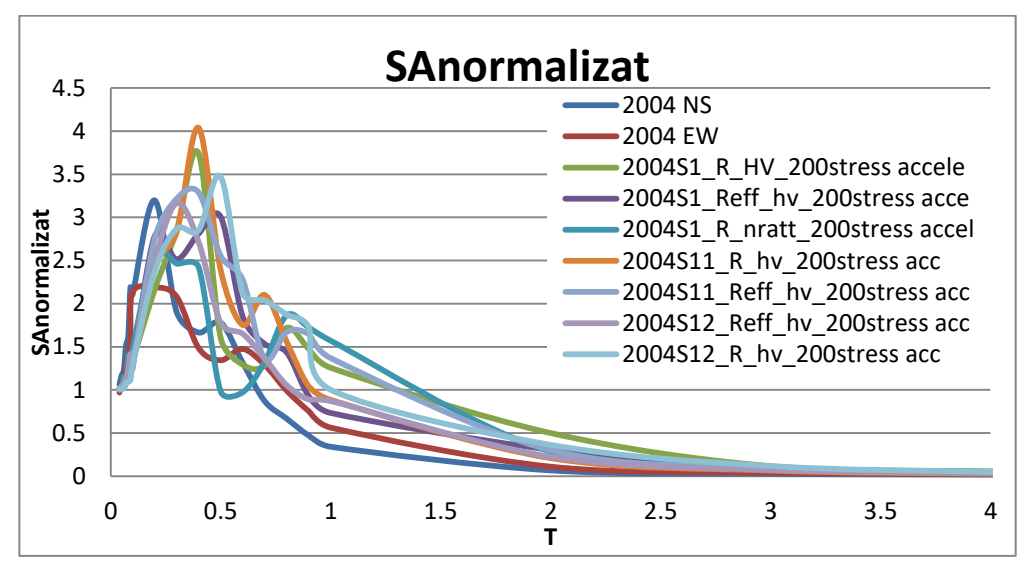


Figure 11. Comparison between the normalized response spectra of the simulations and of the ground motions recorded during the earthquake of October 27, 2004 at INCERC station

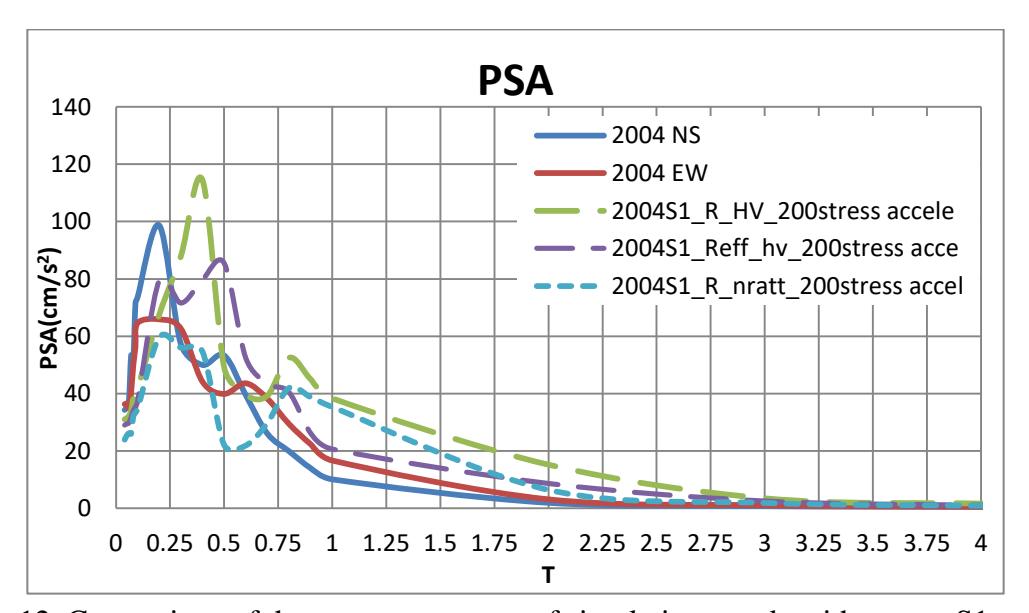


Figure 12. Comparison of the response spectra of simulations made with source S1 and of the ground motions recorded during the earthquake of October 27, 2004 at INCERC station

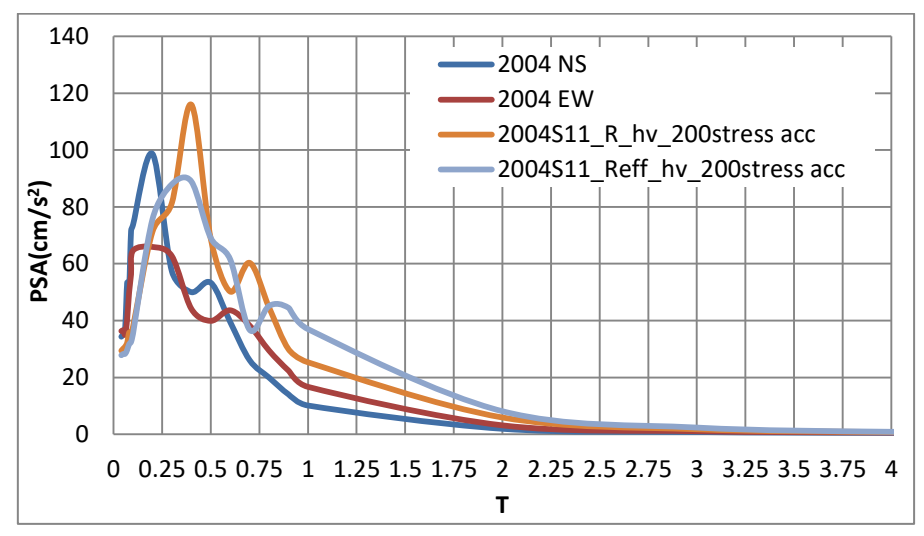


Figure 13. Comparison of the response spectra of simulations made with source S11 and of the ground motions recorded during the earthquake of October 27, 2004 at INCERC station

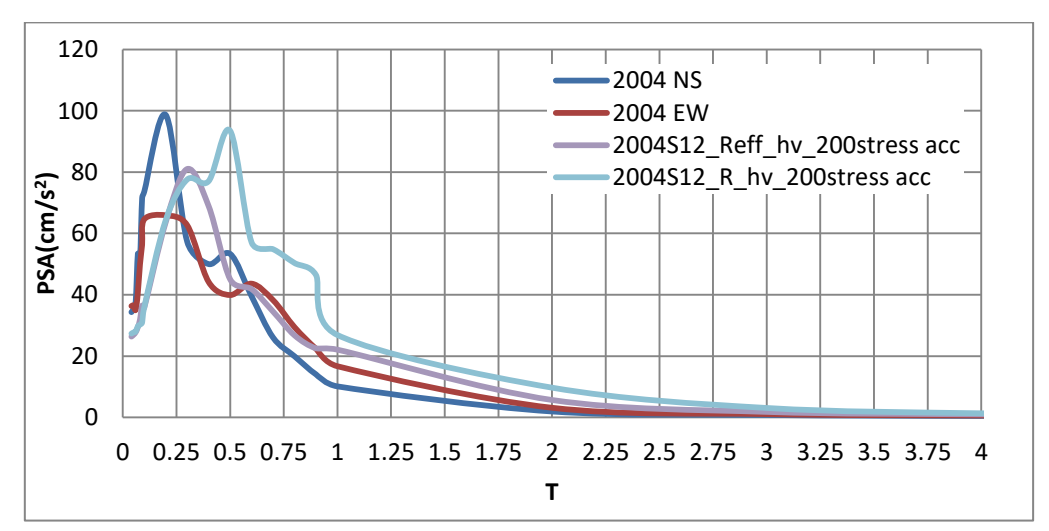


Figure 14. Comparison of the response spectra of simulations made with source S12 and of the ground motions recorded during the earthquake of October 27, 2004 at INCERC station

### **6.3.** The second set of simulations. SMSIM simulations without the influence of local site conditions

In order to observe more easily the changes in the frequency content of the ground motion simulations, there were made a second set of simulations without the amplification given by the local site conditions for the reference distance of 188 km.

#### Conclusions:

- 1. The arithmetic mean of peak acceleration on the 400 simulations for each source type are 7.50 cm/s<sup>2</sup> for S1, 8.08 cm/s<sup>2</sup> for S11 and 6.10 cm/s<sup>2</sup> for S12. The amplifications given by local field conditions increase the amplitudes of the movements by 3.5-4 times.
- 2. There remains a tendency to decrease the peak accelerations of the source 12 (multiplicative spectrum).

- 3. As expected, the frequency content is not altered by the amplification of local field conditions.
- 4. It is observed that the S12 source approaches as a normalized spectrum of recorded motion in the EW direction, although it fails to capture the amplifications for short periods.

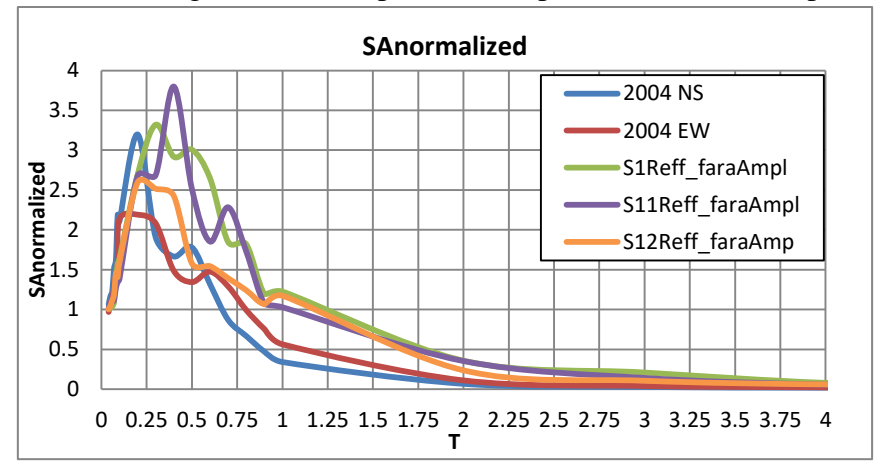


Figure 15. Comparison of normalized response spectra of simulations without the influence of local site conditions and of the ground motions recorded during the earthquake of October 27, 2004 at INCERC station

#### 6.4. The third set of simulations. SMSIM simulations near source

The third set of simulations is performed for a distance of  $R=1\ km$  (near the source), eliminating the effects of the path from source to site.

It is observed how the frequency content is affected by the path from source to site, amplifying the movement over a larger spectrum of frequencies, with the tendency to amplify short periods.

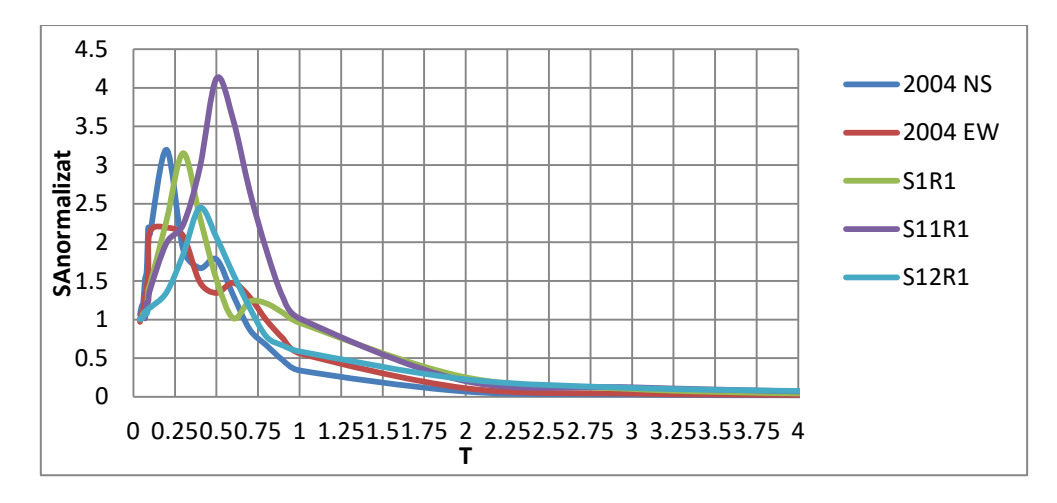


Figure 16. Comparison of normalized response spectra of simulations near the source and of the ground motions recorded during the earthquake of October 27, 2004 at INCERC station

### 6.5. The fourth set of simulations. SMSIM simulations near source for a stress drop of 75 bars and one of 200 bars

Since the stress drop parameter controls the motion frequency content quite enough and the initial simulation set was made by its variation, the four simulation set contains motions near the source with the stress drop values of 75 bars and 200 bars.

#### Conclusions:

- 1. It can be noticed that for a lower value of stress drop Source 12 manages to capture quite well the 2004's earthquake spectra.
- 2. Two frequency corner sources are more influenced by stress drop change.
- 3. Sources S1 and S12 show an increase in the duration of sources with the decrease of stress drop (from 1.37 s to 1.91 s for S1 and from 1.78 to 1.94 s for S12). For source S11 the source duration remains almost constant.
- 4. Decreasing the stress drop also causes a decrease in corner periods.
- 5. The stress drop parameter controls the frequency spectrum of the source spectrum, the use of the 75 bars value makes the peak of the spectral amplitude to be lower (closer to reality).

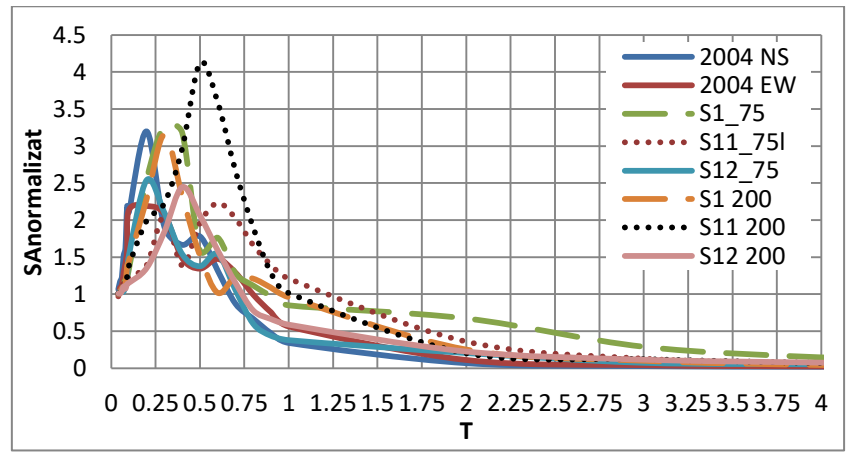


Figure 17. Comparison of the normalized response spectra of simulations near the source with stress drops of 75 bars and 200 bars and of the ground motions recorded during the

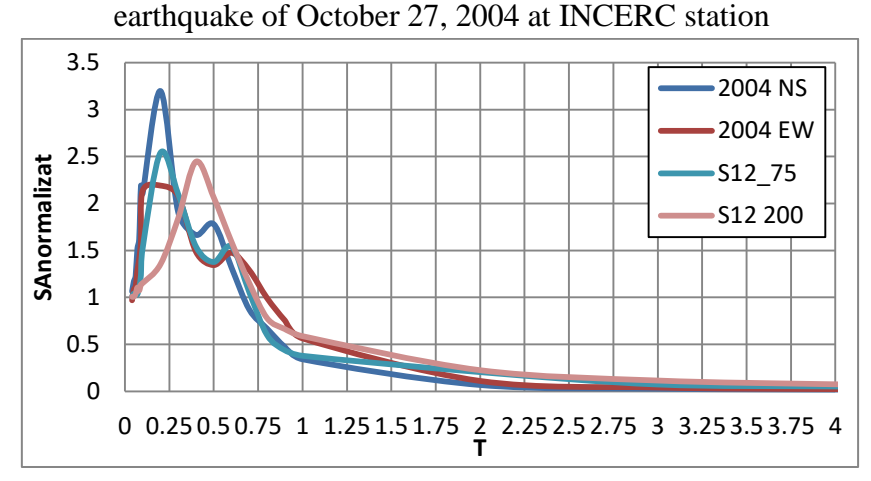


Figure 18. Comparison of the normalized response spectra of S12 simulations near the source with stress drops of 75 bars and 200 bars and of the ground motions recorded during the earthquake of October 27, 2004 at INCERC station

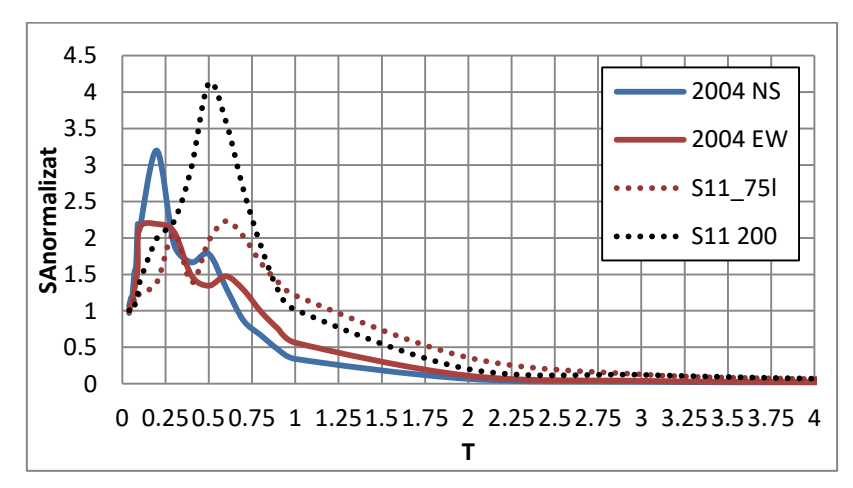


Figure 19. Comparison of the normalized response spectra of S11 simulations near the source with stress drops of 75 bars and 200 bars and of the ground motions recorded during the earthquake of October 27, 2004 at INCERC station

#### **6.6.** The fifth set of simulations.

Simulation sets for source S12 were resumed using a 75 bars value for the stress drop. In the first set of simulations a geometric scattering of  $R^{(-0.5)}$  was used according to Pavel and Vacareanu (2015), but this scattering is more suitable for large earthquakes Mw> 6.9, and the 2004 earthquake is a medium earthquake. The geometric spread for small and medium earthquakes is larger than for large ones, so for the geometric scattering it was used  $R^{(-0.4)}$ . Also, in the attempt to increase the significant duration of the simulations, the path duration was increased to 0.09.

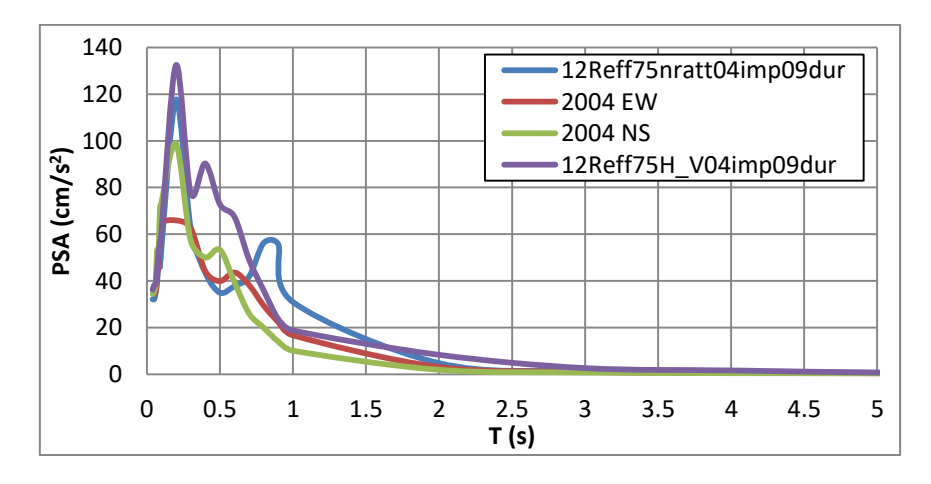


Figure 20. Comparison between the simulated response spectra using source S12, geometric scattering 0.4 and path duration 0.09 and of the ground motions recorded during the earthquake of October 27, 2004 at INCERC station

#### Conclusions:

- 1. Source 12 with a stress parameter of 75 bars conveniently approximates the motion for small periods.
- 2. Modifying the scattering leads to the increase of the average square root, practically the last simulations have a power 3 times greater than the actual earthquake.
- 3. Local site conditions influence the actual duration quite a lot.

- 4. The duration of the source and the duration of the path increased due to the stress modification, respectively the geometric scattering.
- 5. Local amplifications in which the H/V profile was used have overestimated the motion.

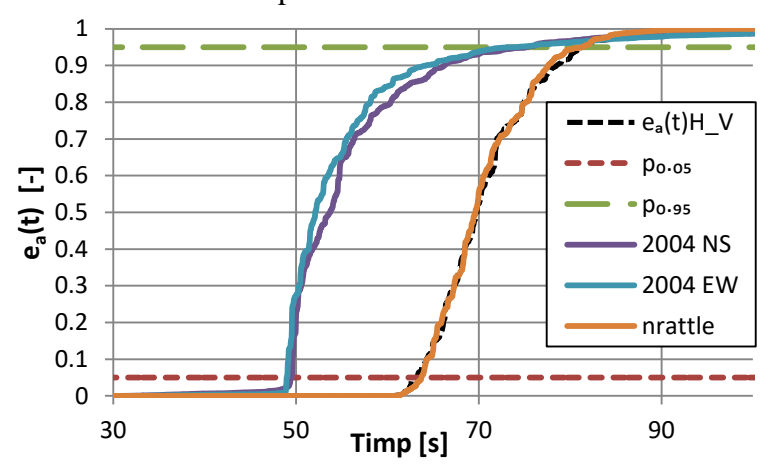


Figure 21. Comparison between the cumulative energies of simulations and those of the ground motions recorded during the earthquake of October 27, 2004 at INCERC station

Type of simulation using SMSIM	Effective duration	Average square root	PGA (cm/s <sup>2</sup> )	Source duration	Path duration	Total duration	fa (Hz)	fb (Hz)	Obs.
INCERC 2004 NS	21.39	3.8	30.01				0.35	0.35	*f <sub>0</sub> cf.
INCERC 2004 EW	20.92	3.4	29.72				0.35	0.35	Gusev et al 2002
Sursa12 Reff H/V 0.4 scattering 0.9 path duration	11.55	9.27	35.14	1.94	16.92	18.86	0.33	1.15	
Sursa12 Reff nrattle 0.4 scattering 0.9 path duration	17.54	8.41	29.91	1.94	16.92	18.86	0.33	1.15	
Sursa1 R nrattle initial parameters	15.93	5.9	22.59	1.37	15.88	17.26	0.726	0.726	
Sursa12 Reff H/V initial parameters	14	7.4	25.42	1.32	16.31	17.64	0.5	1.5	

Table 4. The characteristics of the simulated motions for a stress drop of 75 bars

#### **6.7.** The sixth set of simulations. Window function

In SMSIM the shape of the accelerogram is controlled by a box or exponential window. The shape distribution of the motion in time greatly influences the effective duration and the average square root. In this set of simulations a more appropriate window was sought.

						Significant
Window	eps	eta	ftb	ftext	arms	duration
original	0.20	0.05	2.00	1.00	8.41	17.57
disertatie	0.09	0.05	1.50	1.00	9.14	13.22
1	0.08	0.05	2.00	1.00	7.66	18.14
2	0.08	0.02	2.00	1.00	8.65	14.15
3	0.10	0.001	3.00	1.00	7.79	15.27
4	0.07	0.001	3.00	1.00	9.67	12.88
5	0.06	0.05	2.00	1.00	7.70	17.69
6	0.06	0.04	4.00	0.58	6.11	30.89
7	0.05	0.08	19.00	0.10	5.88	30.56
8	0.09	0.08	19.00	0.10	6.05	30.56
9	0.05	0.00	2.00	1.00	7.40	19.50
10	0.05	0.09	2.00	1.00	7.30	19.63
11	0.08	0.15	2.00	1.00	6.87	23.63
12	0.08	0.15	1.00	1.00	10.80	10.67
13	0.10	0.15	2.00	1.00	10.73	10.75
17	0.30	0.05	2.00	7.00	7.26	16.17
22	0.10	0.05	2.00	7.00	7.59	17.47
23	0.01	0.05	2.00	7.00	7.62	17.89
24	0.01	0.10	2.00	7.00	6.70	23.30
25	0.01	0.20	2.00	7.00	5.80	31.00
26	0.01	0.20	1.00	7.00	8.30	16.50
27	0.01	0.40	0.50	9.00	8.60	16.50
28	0.01	0.60	0.50	7.00	6.50	25.00
14	0.3	0.05	0.1	7	38	0.73
15	0.3	0.05	0.2	7	32	1.9
16	0.3	0.05	0.5	7	13.68	4.36

Table 5. Types of window parameters

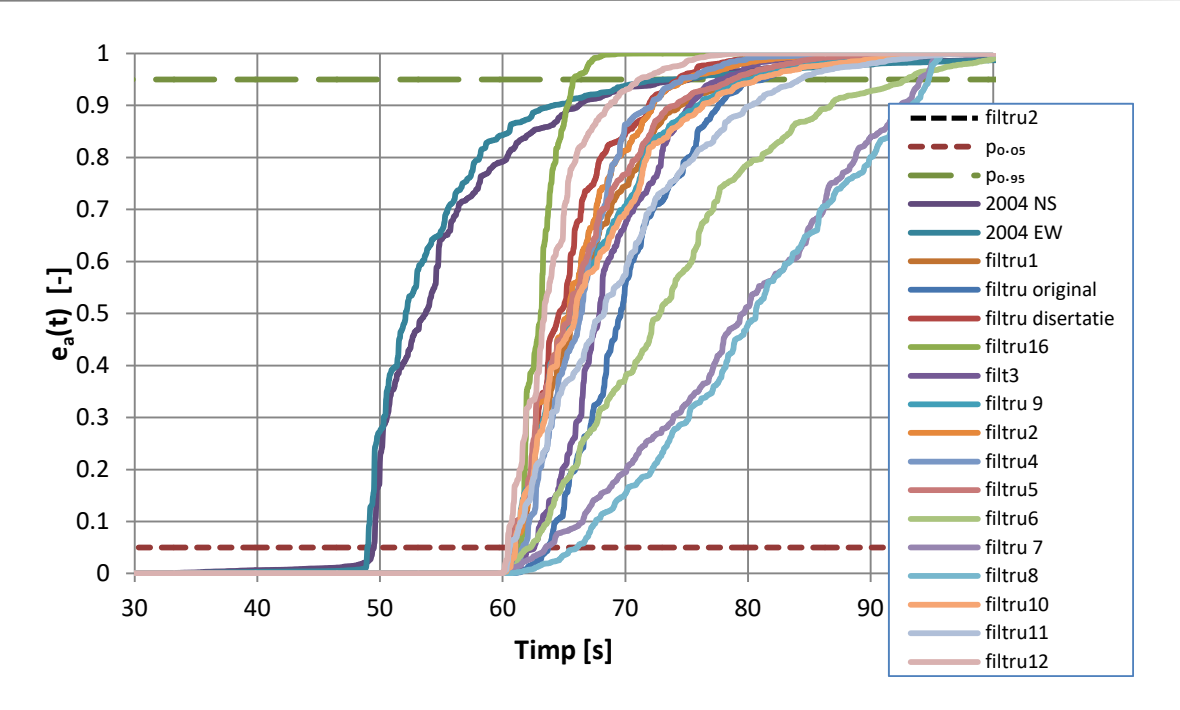


Figure 22. Comparison between the cumulative energies of simulations with different parameters for the window and those of the ground motions recorded during the earthquake of October 27, 2004 at INCERC station (first part)

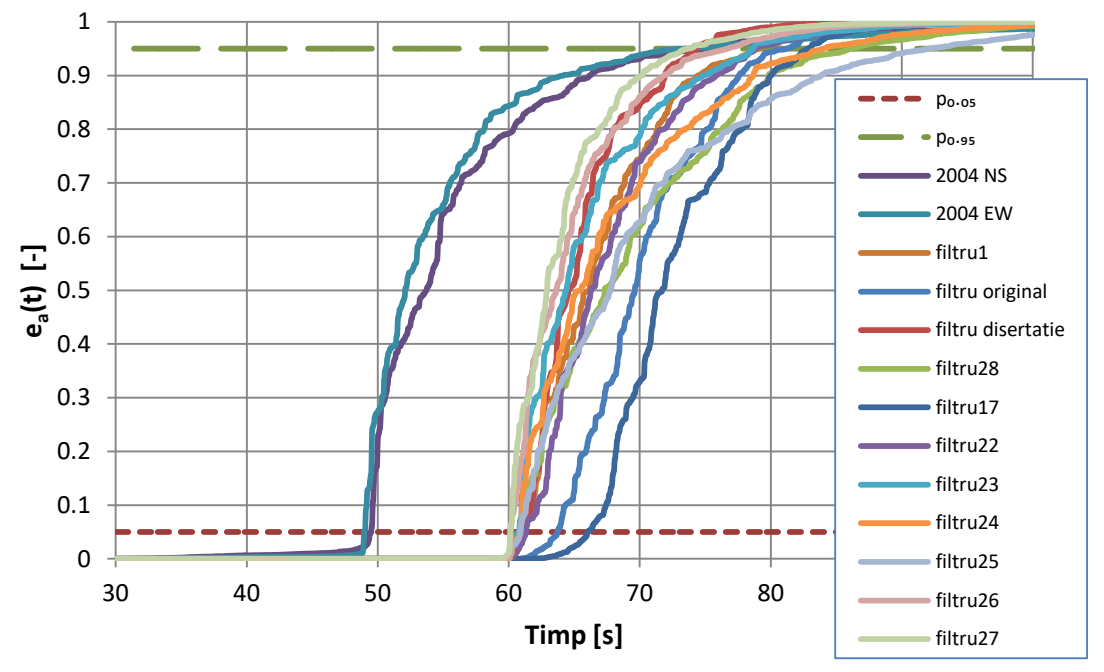


Figure 23. . Comparison between the cumulative energies of simulations with different parameters for the window and those of the ground motions recorded during the earthquake of October 27, 2004 at INCERC station (second part)

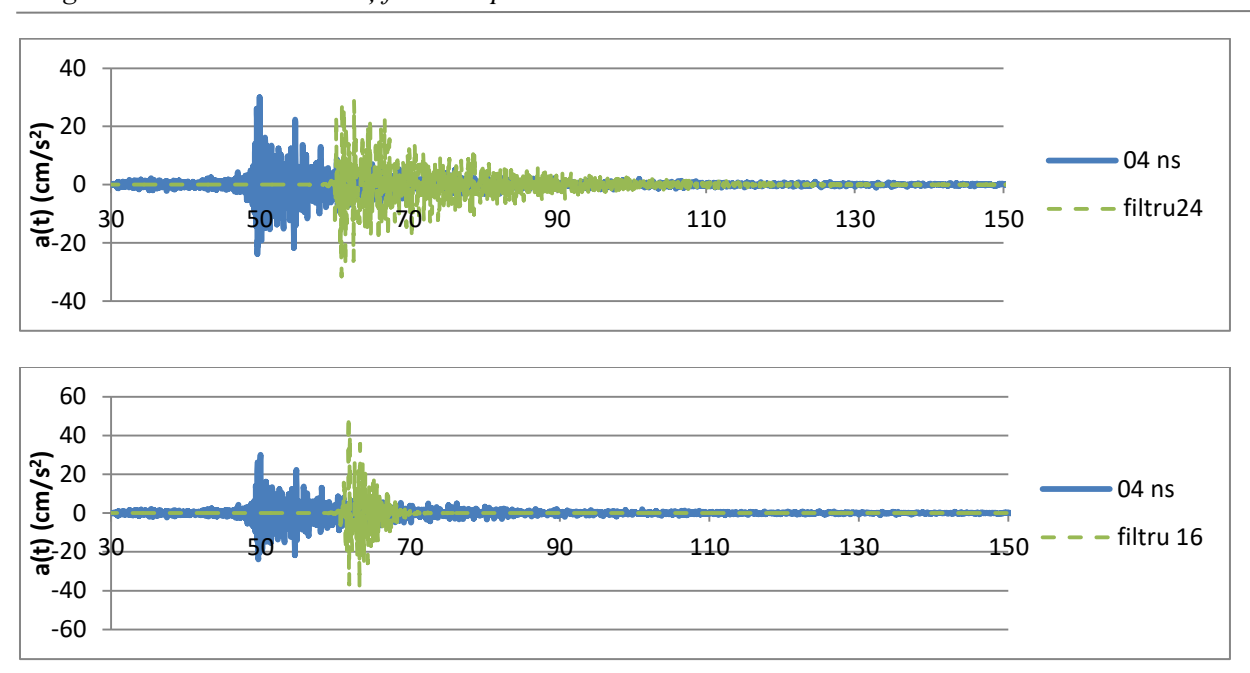


Figure 24. Comparison between the simulated accelerograms using window 16 and 24 and the NS INCERC accelerogram recorded on October 27, 2004

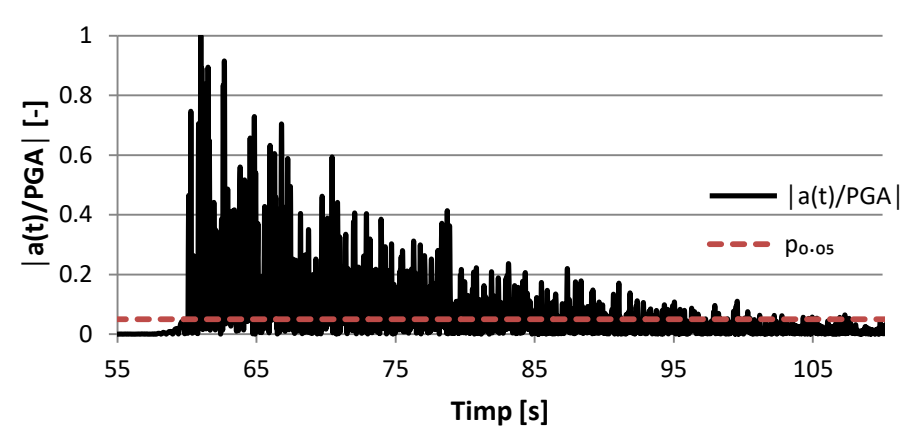


Figure 25. Normalized accelerogram simulated with window 24

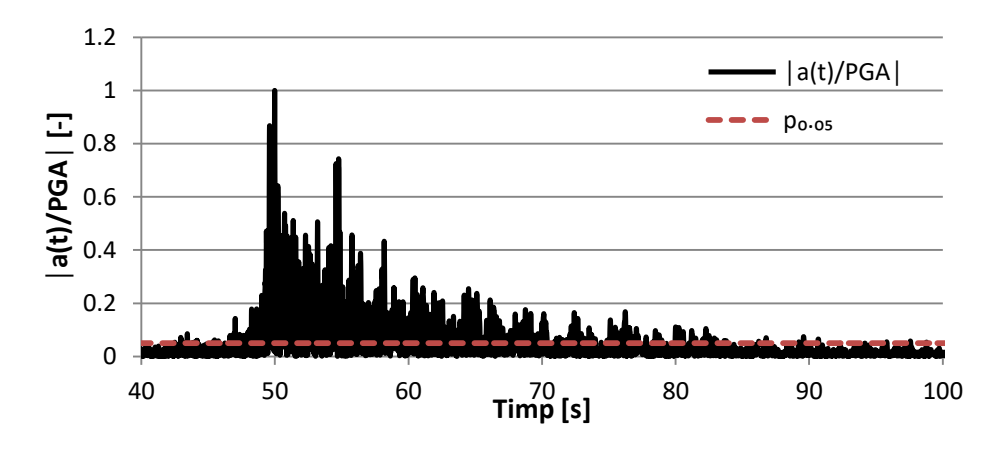


Figure 26. NS INCERC normalized accelerogram recorded on 27 octombrie 2004

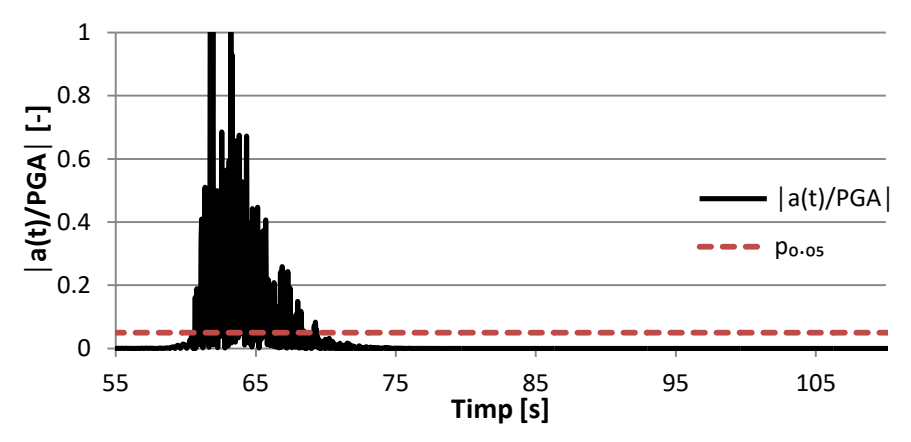


Figure 27. Normalized accelerogram simulated with window 16

It has been found that the exponential window implemented in the SMSIM fails to lead to the specific form of the ground motions produced by subcrustal Vrancean earthquakes, which has a first pulse type motion that contains approximately 35% of the total energy, and a long tail that releases the rest of the energy slowly. The window gives eighter a sudden release of energy or a slow release. To be able to describe the Vrancea produced specific ground motions, a new window will be needed. The window should define the energy release through two slopes.

#### **6.8.** Final set of simulations.

In SMSIM, the accelerogram shape is controlled by a box or exponential filter. It greatly influences the effective duration and the average square root. In this set of simulations, it was used an exponential window from Boore's paper (2003), in which  $\epsilon=0.01$ ,  $\eta=0.1$ , ftb = 2.0, ftext = 7.0. The scatter remained at 0.4, the path duration was taken 0.09 and the stress drop 75 bar.

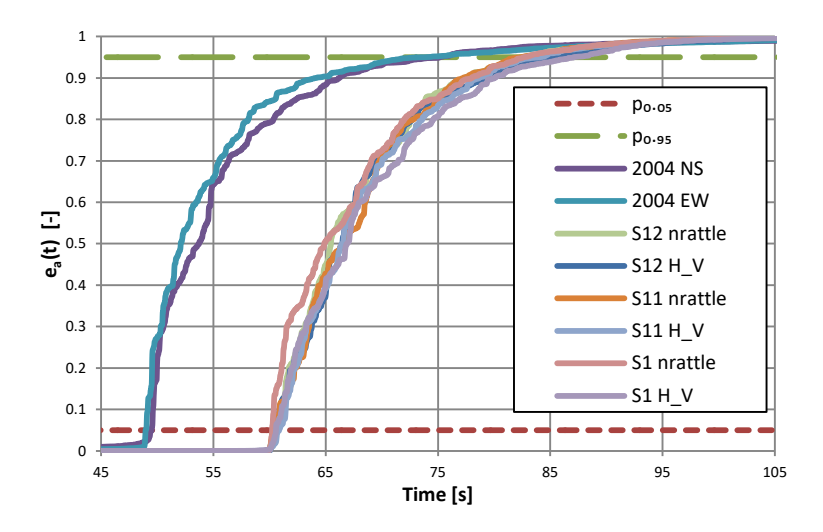


Figure 28. Comparison between the simulated cumulative energies of the final version and those of the ground motions recorded during the earthquake of October 27, 2004 at INCERC station

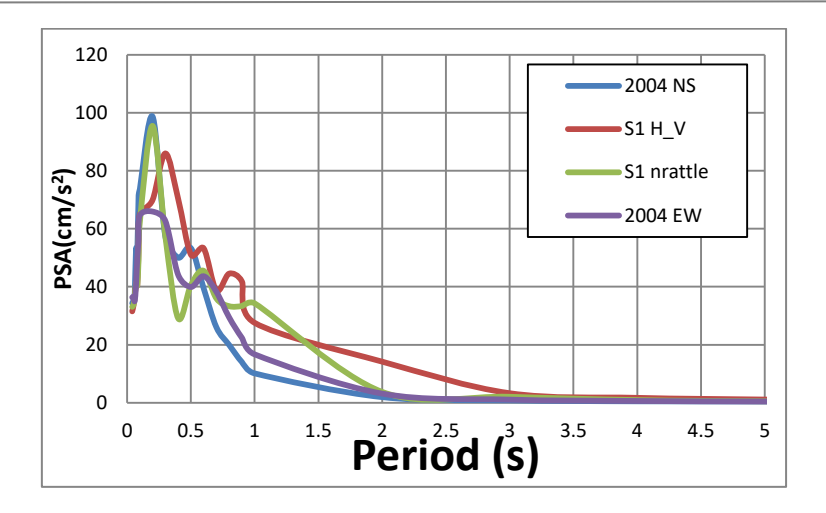


Figure 29. Comparison of the response spectra of simulated accelerograms and those of the ground motions recorded during the earthquake of October 27, 2004 at INCERC station

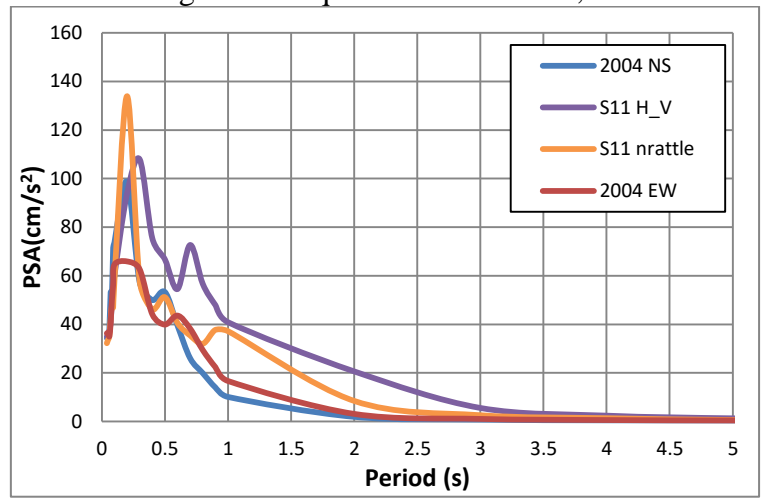


Figure 30. Comparison of the response spectra of simulated accelerograms and those of the ground motions recorded during the earthquake of October 27, 2004 at INCERC station

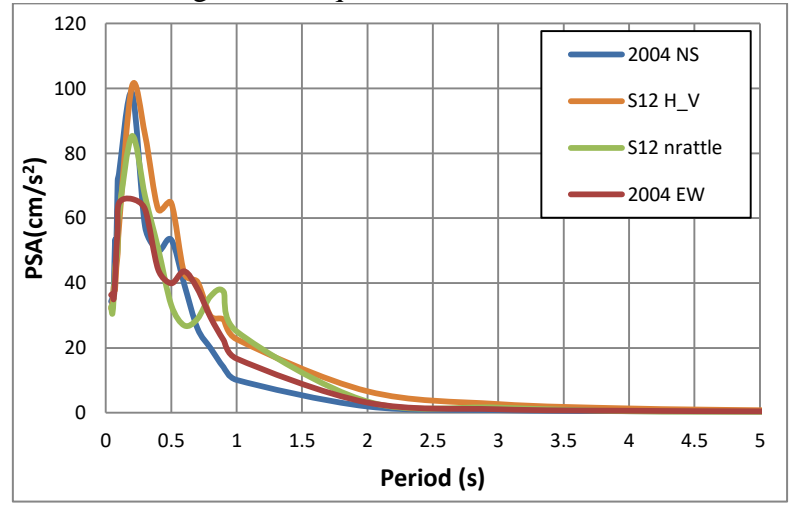


Figure 31. Comparison of the response spectra of simulated accelerograms and those of the ground motions recorded during the earthquake of October 27, 2004 at INCERC station

#### Conclusions:

- 1. From the point of view of released energy, all sources have a power approximately 2 times greater than the normal earthquake.
- 2. The actual time of the simulations is also higher than the real one.
- 3. The amplification of the H/V profile for sources S1 and S11 increases the period at which the first spectral acceleration peak is found.
- 4. For sources S1 and S11, there is an increase greater than the real one for long periods.
- 5. From the point of view of the average of the peak accelerations on the 400 simulations, an oversize of movement can be observed, which may be due to the energy release difference given by the chosen filter, or due to the chosen geometric sprading.
- 6. In theory, a smaller earthquake has a larger geometric spreading, but the scatter modification for the last simulations was chosen without a research.
- 7. Using a more suitable filter and scaling modification based on more detailed research would most likely lead to a better fit of the simulation

Type of simulation using SMSIM	Average PGA	PGA of the analyzed simulation	fa (Hz)	fb (Hz)	Source duration	Path duration	Total duration	Significant duration	Average square root
S1 H_V	39.68	29.82	0.523	0.523	1.91	16.92	18.83	22.88	7.92
S1 nrrattle	33.13	30.86	0.523	0.523	1.91	16.92	18.83	22.4	7.08
S11 H_V	42.73	33.56	0.33	0.82	1.51	16.92	18.43	23.97	9.40
S11 nrattle	34.8	29.62	0.33	0.82	1.51	16.92	18.43	21.95	7.99
S12 H_V	36.41	31.08	0.33	1.15	1.94	16.92	18.86	25.04	7.39
S12 nrattle	31.23	29.39	0.33	1.15	1.94	16.92	18.86	22.11	6.78

Table 6. Characteristics of simulated ground motion of 27 October 2004 for a 75 bars stress drop, geometric spreading of 0.4 and path time 0.09

# 7. Simulations of the ground motion generated by the intermediate depth earthquake in August 30, 1986 at INCERC station. Interpretation of results

#### 7.1. Earthquake characteristics

The earthquake of August 30th 1986 was a large sized one with a magnitude of 7.1 at a depth of 131.4 km, its epicenter being  $45.52^{\circ}$  N and  $26.49^{\circ}$  E longitude (ROMPLUS - Radulian et al. 2019). The seismic fault dimensions according to 0th et al. (2007) were  $12.8 \times 12.6$  km and the stress drop was 50 bars (Gusev et al. 2002, Oncescu and Bonjer 1997). The strike angle was  $227^{\circ}$ , the dip  $65^{\circ}$  and the rake  $104^{\circ}$  (Ganas et al. 2010).

#### 7.2. Input parameters

The average velocity of the shear waves and the density in the vicinity of the source were considered 4.5 km/s and 2.8 g/cm<sup>3</sup> (Martin and Wenzel 2006, Sokolov et al. 2008).

Three types of spectra were investigated for the point-source simulations (SMSIM): one-corner frequency source (S1), two-corner frequencies source with multiplicative spectrum

(S11) and additive spectrum (S12) defined according to Boore (2003). For the hypocentral distance the effective distance (Reff) that accounts for the fault geometry was used (182.2 km). The geometrical scattering, attenuation and kappa spectral degradation parameters were considered according to Pavel and Vacareanu (2015).

The simulations are made for the INCERC seismic station, Bucharest. For the linear behavior of soil, two amplification types were considered: the local site amplifications determined using NRATTLE (subprogram from the SITEAMP, SMSIM collection) and the local site amplifications taken from the paper of Pavel (2015) and determined with the H/V ratio method. Window 16 was used in the simulations.

	7.5. Characteristics of Simulations											
Type of simulation using SMSIM	Average PGA (cm/s <sup>2</sup> )	PGA of the analyzed simulation (cm/s <sup>2</sup> )	fa (Hz)	fb (Hz)	Source duration	Path duration	Total duration	Significant duration	Average square root			
1986 NS*		95.3	0.13	0.13				16.19	19.47			
1986 EW*		88.7	0.13	0.13				13.35	23.86			
S1 H_V	69.82	88.66	0.1	0.1	9.7	15.81	25.51	13.86	22.11			
S1 nrrattle	49.27	59.52	0.1	0.1	9.7	15.81	25.51	14.38	16.74			
S11 H_V	73.02	90.14	0.07	0.14	6.74	15.81	22.55	14.21	23.09			
S11 nrattle	51.25	65.25	0.07	0.14	6.74	15.81	22.55	14.3	15.26			
S12 H_V	69.64	89.88	0.07	0.29	8.45	15.81	24.26	14.94	20.34			
S12 nrattle	49.53	66.36	0.07	0.29	8.45	15.81	24.26	13.64	15.53			

**7.3.** Characteristics of simulations

Table 7. Characteristics of simulated ground motion of August 1986's earthquake using SMSIM

For each source definition, 400 accelerograms were generated using SMSIM with the two types of amplifications for the linear soil behavior.

#### Conclusions:

- 1. As one can see from Table 7, the average peak values of the 400 simulations for each case are significantly smaller than the real case. The peak values of the simulations in which the NRATTLE local amplification profile was used are about 30% lower than those in which the H/V amplification profile was employed.
- 2. In terms of significant duration, there is a difference of 1-2s from the recorded ground motion in the NS direction and a good match with EW direction is observed. Given the differences between peak accelerations obtained using NRATTLE and H/V amplification profile simulations, it can be noted that the root mean square values of the simulations and of the real event are roughly the same.
- 3. Regarding the frequency content, the NRATTLE amplitude profile largely underestimates the ground motion for long periods and for periods in the range of 0.4-0.6s. The H/V

<sup>\*</sup> f<sub>a</sub> and f<sub>b</sub> were determined according to Gusev et al. (2002)

- profile manages to capture an amplification of the ground motion for long periods for the cumulative source spectra.
- 4. For all types of simulations, a peak of the spectral amplitudes remained around the 0.2-0.3s period, most likely because the simulations did not considered the nonlinear behavior of the soil. S11 and S12 sources estimate better the real seismic ground motion.

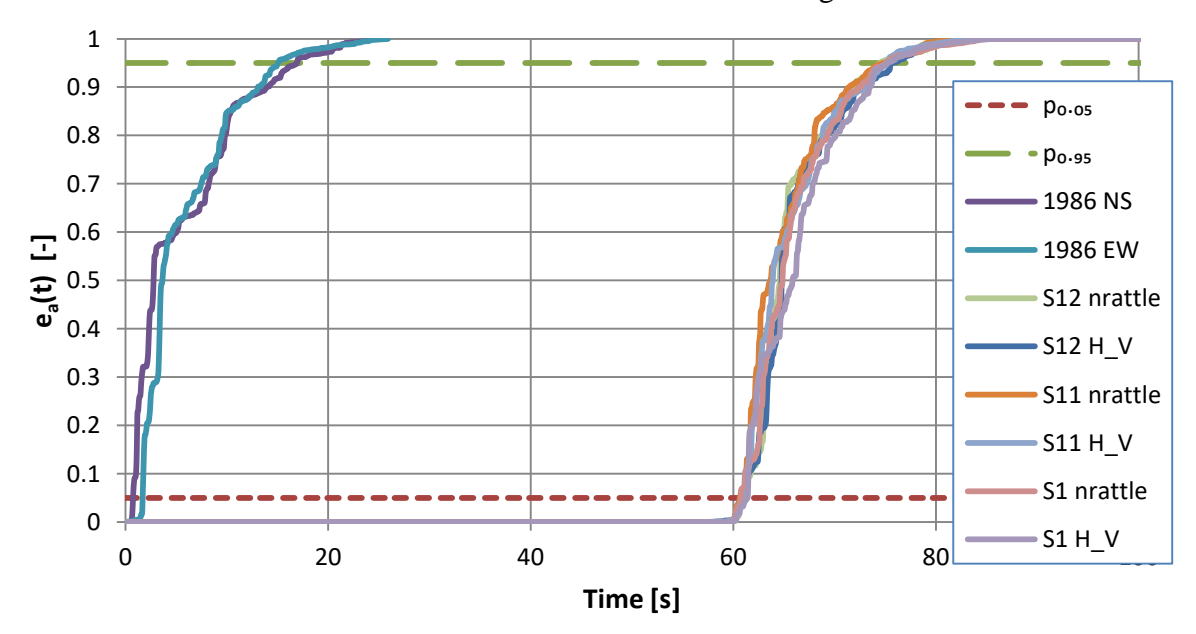


Figure 32. Cumulative energies of recorded ground motions and simulations made with SMSIM with NRATTLE and H/V soil profile amplification

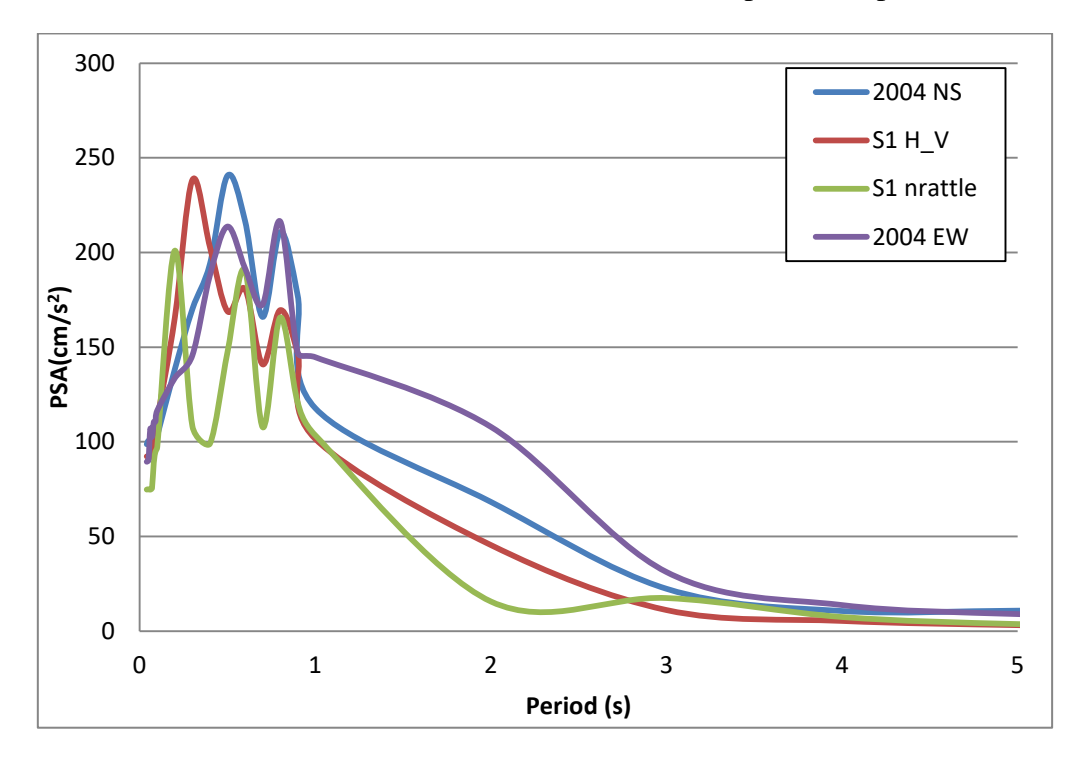


Figure 33. Comparison of the response spectra of simulations made with SMSIM source S1 and of recorded ground motions on August 30, 1986's Vrancea earthquake, INCERC seismic station

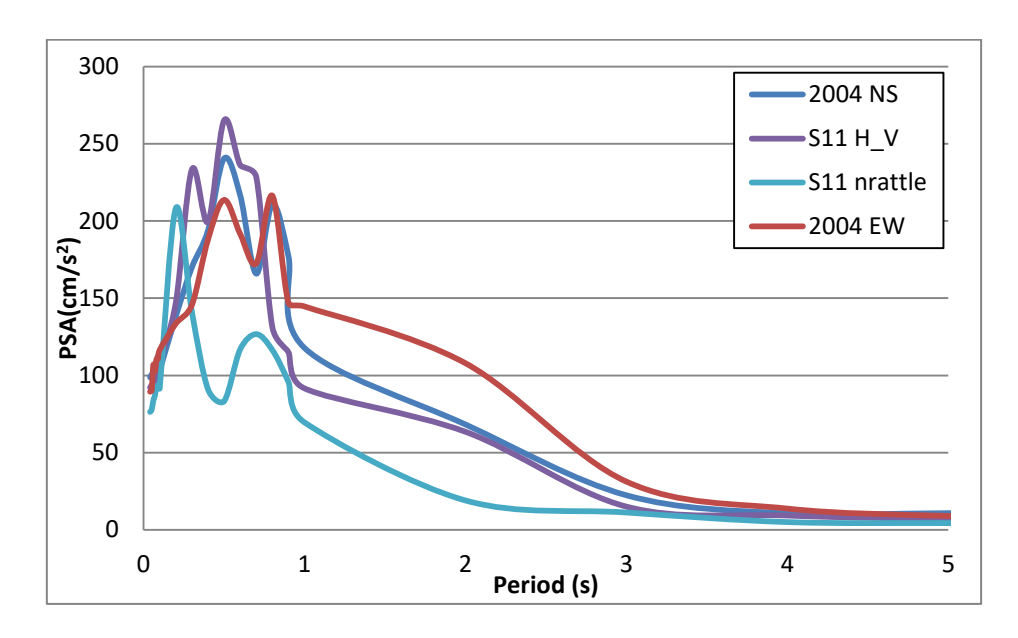


Figure 34. Comparison of the response spectra of simulations made with SMSIM source S11 and of recorded ground motions on August 30, 1986's Vrancea earthquake, INCERC seismic station

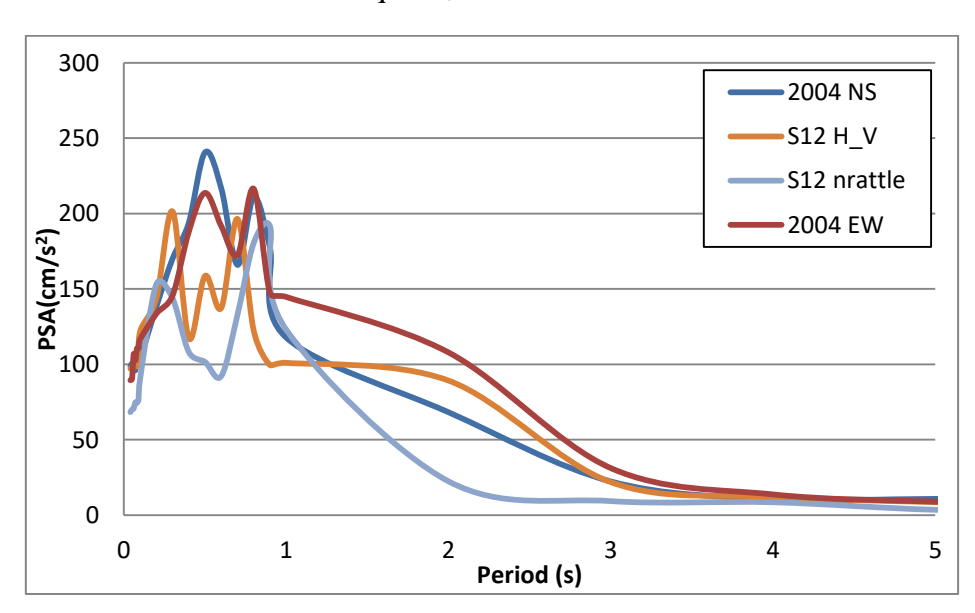


Figure 35. Comparison of the response spectra of simulations made with SMSIM source S12 and of recorded ground motions on August 30, 1986's Vrancea earthquake, INCERC seismic station

#### 8. Conclusion. Pros and cons

Simulations were performed for INCERC station site for two intermediate depth earthquakes: October 27, 2004 (medium event) and August 30, 1986 (large event) using the SMSIM set of programs version 7.1 (Boore, 2005). The ground motions were simulated for 3 types of spectral source (with a single corner frequency, and with two corner frequencies with multiplicative and additive spectrum) and two types of amplification of local site conditions (one calculated with NRATTLE program and the other with H/V method).

The following were noted:

- a. The stress drop parameter changes the peak values of the motion, the frequency content and the duration of the source.
- b. The use of effective distance  $R_{\text{eff}}$  that takes into account the focal mechanism leads to a better approximation of the seismic motion.
- c. Significant durations and root mean square accelerations are very sensitive to the used window.
- d. The root mean square acceleration is also significantly influenced by the amplification profile used.
- e. Geometric scattering greatly influences the peak values of the motions.
- f. For a form of the motion in which high energy is initially released in a short time, and the rest of the energy is released gradually and slower, a two-interval window with two slopes would be required.
- g. For the 2004 earthquake the simulations performed with the NRATTLE amplification profile estimate quite well the motion for all three types of sources. The simulations performed with the H/V profile tend to modify the amplification peaks for longer periods.
- h. For the 2004 earthquake, source 12 is least influenced by the amplification profile of local site conditions.
- i. Because for the 1986 earthquake, a more appropriate window was defined, the significant durations and the root mean square accelerations coincide approximately. In the case of the simulations performed for the 2004 earthquake, the mismatch is probably due to the mismatch of the window and the modification of the geometric scattering.
- j. For large earthquakes, the program does not capture the non-linear behavior of the land.

In conclusion, the program simulates fairly well the medium earthquakes that do not produce soil nonlinear behavior, but for large earthquakes it is necessary to use another program that takes into account the nonlinearity of the ground (eg. DEEPSOIL), the simulations are sensitive to the choice of the noise modeling window, and it fails to capture the two types of energy release. The input parameters must be chosen after appropriate studies because they can produce quite major changes in the characteristics of the simulated motions.

#### **Biography**

- 1. Boore DM (2003) Simulation of ground motion using the stochastic method. Pure Appl Geophys 160:635–676
- 2. Boore DM (2005) SMSIM—Fortran programs for simulating ground motions from earthquakes: version 2.3—a revision of OFR 96-80-A. U.S. Geological Survey Report OFR 00–509
- 3. Boore DM, Joyner WB (1997) Site amplifications for generic rock sites. Bull Seismol Soc Am 87(2):327–341
- 4. Boore, D. M. (1983). Stochastic simulation of high-frequency ground motions based on seismological models of the radiated spectra, Bull. Seismol. Soc. Am. 73, 1865–18943
- 5. http://www.daveboore.com/software\_online.html
- 6. Brune, J. N. (1970). Tectonic stress and the spectra of seismic shear waves from earthquakes, J. Geophys. Res. 75, 4997–5009.
- 7. Brune, J. N. (1971). Correction, J. Geophys. Res. 76, 5002
- 8. Irikura K., Miyake H. Lecture note on Strong Motion Seismology
- 9. ATKINSON, G. M. (1996), The High-frequency Shape of the Source Spectrum for Earthquakes in Eastern and Western Canada, Bull. Seismol. Soc. Am. 86, 106–112.
- 10. ATKINSON, G. M. and SILVA, W. (2000), Stochastic Modeling of California Ground Motions, Bull. Seismol.Soc. Am. 90, 255–274.
- 11. Atkinson, G. M. and Silva, W. (1997). An Empirical Study of Earthquake Source Spectra for California Earthquakes. Bull. Seismol. Soc. Am., 87:97–113.
- 12. Atkinson, G. M., and D. M. Boore (2003). Empirical ground-motion relations for subduction zone earthquakes and their application to Cascadia and other regions, Bull. Seismol. Soc. Am. 93, 1703–1729.
- 13. Atkinson Gail M., Karen Assatourians, David M. Boore, Ken Campbell, and Dariush Motazedian, A Guide to Differences between Stochastic Point-Source and Stochastic Finite-Fault Simulations, Bulletin of the Seismological Society of America, Vol. 99, No. 6, pp. 3192–3201, December 2009, doi: 10.1785/0120090058
- 14. Hanks, T. C., and R. K. McGuire (1981). The character of high-frequency strong ground motion, Bull. Seismol. Soc. Am. 71, 2071–2095.
- 15. Motazedian D., Atakinson G.M., Stochastic Finite-Fault Modeling Based on a Dynamic Corner Frequency, Bulletin of the Seismological Society of America, Vol. 95, No. 3, pp. 995–1010, June 2005, doi: 10.1785/0120030207

41

- 16. Hartzell, S. H. (1978). Earthquake aftershocks as Greens functions, Geophys. Res. Lett. 5, 1–4.
- 17. AKI, K. (1967), Scaling Law of Seismic Spectrum, J. Geophys. Res. 72, 1217–1231.
- 18. ANDERSON, J. G. and HOUGH, S. E. (1984), A Model for the Shape of the Fourier Amplitude Spectrum of Acceleration at High Frequencies, Bull. Seismol. Soc. Am. 74, 1969–1993.
- 19. Sokolov, V., Bonjer, K.-P., Onescu, M., and Rizescu, M. (2005). Hard Rock Spectral Models for Intermediate Depth Vrancea (Romania) Earthquakes. Bull. Seismol. Soc. Am., 95:1749–1765.
- 20. Sperner, B., Lorenz, F. P., Bonjer, K.-P., Hettel, S., Müller, B., and Wenzel, F. (2001). Slab Break-off Abrupt Cut or Gradual Detachment? New Insights from the Vrancea Region (SE Carpathians, Romania). Terra Nova, 13:172–179.
- 21. Constantinescu, L., Enescu, E., Vrancea earthquakes from scientific and technologic point of view, Editura Academiei, 230p., (in Romanian), 1985
- 22. Oncescu, M. C. and K.-P. Bonjer (1997). A note on the depth recurrence and strain release of large Vrancea earthquakes. Tectonophysics, 272, 291-302.
- 23. Oth A, Parolai S, Bindi D, Wenzel F (2009) Source spectra and site response from S waves of intermediate-depth Vrancea, Romania, earthquakes. Bulletin of the Seismological Society of America 99:235-254
- 24. Martin, M., Wenzel, F., and the CALIXTO working group (2006). High-Resolution Teleseismic Body Wave Tomography Beneath SE-Romania (II): Imaging of a Slab Detachment Scenario. Geophys. J. Int., 164:579–595.
- 25. Wenzel F., Sperner B., Lorenz F., Mocanu V. Geodynamics, tomografic images and seismicity of Vrancea region (SE-Carpatians, Romania), EGU Stephan Mueller Special Publication Series, 3, 95–104, 2002
- 26. Ganas A., Grecu B., Batsi E., Radulian M., Vrancea slab earthquake triggerd by static stress transfer, Nat. Hazards Earth Syst. Sci., 10, 2565–2577, 2010, doi:10.5194/nhess-10-2565-2010
- 27. V. Sokolov · K P Bonjer . F. Wenzel · B. Grecu, M. Radulian, Ground-motion prediction equations for the intermediate depth Vrancea (Romania) earthquakes, Bull Earthquake Eng (2008) 6:367–388 DOI 10.1007/s10518-008-9065-6
- 28. Oth A, Bindi D, Parolai S, Wenzel F (2008) S-wave attenuation characteristics beneath the Vrancea region in Romania: new insights from the inversion of ground-motion spectra. Bull Seismol Soc Am 98(5):2482–2497
- 29. Oth A., Wenzel F., Radulian M., Source parameters of intermediate-depth Vrancea (Romania) earthquakes from empirical Green's functions modeling, Tectonophysics 438 (2007) 33–56

- 30. Pavel F, Vacareanu R (2015) Kappa and regional attenuation for Vrancea (Romania) earthquakes. J Seismol. doi:10.1007/s10950-015-9490-3
- 31. Pavel F., Investigation on the stochastic simulation of strong ground motions for Bucharest area, Soil Dynamics and Earthquake Engineering 69 (2015) 227–232
- 32. Radulian M, Popa M, Carbunar OF, Rogozea M (2008) Seismicity patterns in Vrancea and predictive features. Acta Geodaetica et Geophysica Hungarica 43:163–173
- 33. Pavel F., Ciuiu D., Vacareanu R., Site Dependent Seismic Hazard Assessment for Bucharest Based on Stochastic Simulations, The 1940 Vrancea Earthquake. Issues, Insights and Lessons Learnt Part of the series Springer Natural Hazards pp 221-233,
- 34. P100-1/2013 Cod românesc de proiectare seismică. Ministerul Dezvoltării Regionale și Administrației Publice, București România.
- 35. Radulian M., Mândrescu M.N., Panza G.F., Popescu E. and Utale A., 2000. Characterization of seismogenic zones of Romania, Pure Appl. Geophys., 157, 57–77.
- 36. Constantinescu L., Marza V.I. (1980). A computer-compiled and computer-oriented catalogue of Romania's earthquakes during a millennium (AD 984-1979), Rev. Roum. Geophys. 24, 193 234